https://doi.org/10.5194/gmd-2020-126
Preprint. Discussion started: 4 August 2020


Geoscientific Model Development Discussions
Open Access
EGU

# Sensitivity analysis of the PALM model system 6.0 in the urban environment

Michal Belda[1], Jaroslav Resler[2], Jan Geletič[2], Pavel Krč[2], Björn Maronga[3], Matthias Sühring[3], Mona Kurppa[6], Farah Kanani-Sühring[3,4], Vladimír Fuka[1], Kryštof Eben[2], Nina Benešová[5], and Mikko Auvinen[7]

[1]Department of Atmospheric Physics, Faculty of Mathematics and Physics, Charles University, Prague, Czech Republic
[2]Institute of Computer Science, Czech Academy of Sciences, Prague, Czech Republic
[3]Institute of Meteorology and Climatology, Leibniz University Hannover, Hannover, Germany
[4]Harzenergie GmbH & Co. KG, Goslar, Germany
[5]Czech Hydrometeorological Institute, Prague, Czech Republic
[6]Institute for Atmospheric and Earth System Research / Physics, Faculty of Science, University of Helsinki, Helsinki, Finland
[7]Finnish Meteorological Institute, Helsinki, Finland

**Correspondence:** Michal Belda (michal.belda@mff.cuni.cz)

**Abstract.** Sensitivity of the PALM model 6.0 is tested in a real urban environment in the vicinity of a typical crossroad in a densely built-up residential area in Prague, Czech Republic. Two types of scenarios are employed. First are the synthetic scenarios altering mainly surface and material parameters such as albedo, emissivity or wall conductivity, testing sensitivity of the model simulations to potentially erroneous setting of model inputs. Second, real-life type scenarios are analyzed, in which commonly considered urban heat island mitigation measures are applied, such as greening of the streets or changing surface materials. For the first-type scenarios, surface parameters used in radiation balance equations are found to be the most sensitive overall followed by volumetric heat capacity and thermal conductivity of walls. Other parameters show limited average effect, however, some can still be significant in some parts of the day, such as surface roughness in the morning hours. Second type, the mitigation scenarios, show urban vegetation to be the most effective measure, especially when considering both physical and biophysical temperature indicators. Influence of both type scenarios was also tested for air quality, specifically $PM_{10}$ dispersion which generally shows behaviour opposite to thermal indicators, ie., improved thermal comfort brings deterioration of $PM_{10}$ concentrations.

## 1 Introduction

The urban climate, especially the urban heat island phenomenon (UHI), has been studied for many decades (Oke, 1982; Arnfield, 2003; Souch and Grimmond, 2006; Mills, 2014). In the context of global climate change and extensive urbanization, even with the progressing computing capabilities and geographic information systems (GIS), the investigation of the urban climate

https://doi.org/10.5194/gmd-2020-126
Preprint. Discussion started: 4 August 2020

Geoscientific Model Development Discussions
Open Access EGU

specifics still faces new challenges, such as the need for standardized methods, numerical modelling or the practical applicability of the research (Stewart, 2011; Mills, 2014). Microscale meteorological and climate models have been increasingly used to simulate real city environments and especially the impacts of changes in the city structure on the environmental conditions that affect the inhabitants. For a long time, cities have been known to strongly modify the surface energy balance and atmospheric conditions by trapping the energy in the city causing the UHI (Oke, 1982). In addition to that, global changes of climate, especially global temperature increase, are expected to have a worldwide influence on human society and other natural ecosystems with potential severe impacts (IPCC, 2014a). The increase of heat load in urban areas has been reported to have a substantially harmful effect on public health (Patz et al., 2005; Haines et al., 2006; Ebi, 2011) with an increase of mortality rates (Kovats and Hajat, 2008; Zanobetti et al., 2012). On the other hand, when appropriate adaptation measure are applied, these negative consequences can be mitigated (Gill et al., 2007; Hunt and Watkiss, 2011; Müller et al, 2013; IPCC, 2014b). As the public and the administrative authorities are becoming aware of the problem, so grows the demand for scientifically based urban climate studies, particularly those that can provide reliable projections on city or street-level scale.

In this context, various UHI mitigation measures are being considered, with greening of the environment as a typical example. Application of these measures, however, needs some prior information about their potential effectiveness. For that, it is important to know how sensitive the environment is to the city layout (e.g., building height or street width) and the material-specific parameters used to describe urban surfaces (e.g., reflectivity or roughness). However, these sensitivities cannot be tested independently in a real city. Additionally, many model/physical parameters describing the city environment are only known approximately or are not available at all. Therefore, it is important to know the sensitivity of the results to the uncertainties in the input data, and which parameters are to be gathered with higher priority in data collection campaigns. Sensitivity studies for urban flow models based on computational fluid dynamics (CFD) are rare and typically deal with parameters such as grid size/resolution or the type of turbulence model included (e.g., Ai et al., 2014 or Ramponi and Blocken, 2012). More common are studies that consider the effect of potential changes in urban development, such as tree planting, green roofs or changes of certain surface materials. For example, Ashie and Kono (2010) evaluate the impact of a redevelopment plan in two districts of Tokyo using a RANS-based (Reynolds-averaged Navier-Stokes) CFD model and Gross (2012) considers the effects of various green design elements, such as green facades, green roofs, lawns and trees also using a RANS-based CFD code. Many previous studies have also applied the RANS code called ENVI-met, but the focus was on a small number of specific changes, instead of a systematic model sensitivity study (e.g., Su et al., 2014; Emmanuel and Loconsole, 2015; Lobaccaro and Acero, 2015). Large-eddy simulation (LES) is a branch of CFD in which the large turbulent eddies are explicitly resolved and simulated, unlike RANS where all turbulent eddies are modelled. To the best of our knowledge, systematic sensitivity studies of microclimate models based on the large-eddy simulation method are non-existent.

This paper presents a systematic sensitivity analysis using the LES-based PALM model system (Maronga et al., 2015, 2020). The selected area of interest is based in a real urban district in Prague, Czech Republic. Our interest concentrates on the sensitivity of the air temperature, surface temperature, and $PM_{10}$ (particulate matter larger than 10 $\mu$m in diameter) concentration to the parameters describing the properties of the urban surfaces. Several idealised adaptation measures (e.g., changing surface materials or adding/removing urban greenery) are also considered.

https://doi.org/10.5194/gmd-2020-126
Preprint. Discussion started: 4 August 2020




## 2 Experiment setup

### 2.1 Model description

The PALM model system 6.0 (revision 4093) (Maronga et al., 2015, 2020) consists of the PALM model core, several embedded modules, and PALM-4U (short for PALM for urban applications) components which have been specifically developed for modelling of the urban environment. PALM model core resolves the non-hydrostatic, filtered, incompressible Navier-Stokes equations for wind $(u, v, w)$ and scalar quantities (potential temperature, water vapor mixing ratio, passive scalar) on a staggered Cartesian grid in Boussinesq-approximated form. The sub-grid scale terms that arise from filtering are parametrized using a 1.5-order closure by Deardorff (1980), with modifications after Moeng and Wyngaard (1988) and Saiki et al. (2000). One of the assets of PALM is its excellent scalability for massively parallel computer architectures (up to 50,000 processor cores, see Maronga et al., 2015).

This study applies several modules embedded in PALM, namely the land surface (LSM), plant canopy (PCM) and radiation model. The radiation model applies the Rapid Radiation Transfer Model for Global Models (RRTMG), which has been used as an external library. Furthemore, the following PALM-4U components are applied: the Cartesian topography, building surface model (BSM, formerly USM, see Resler et al., 2017) and radiative transfer model (RTM) (Krč et al., 2020), and human biometeorology and online chemistry modules.

Additionally both self- and offline nesting features of PALM-4U are utilised. Self-nesting means that a domain with a finer resolution can be defined inside a larger domain and this subdomain (child domain) receives its boundary conditions from the coarse-resolution parent domain at every model timestep. In offline nesting, the initial and boundary conditions for the mean flow of the parent domain are provided from, e.g., a mesoscale model using a dynamic driver, while the child domain receives all information from its parent. As offline nesting is usually used for coupling to a large-scale or mesoscale model that does not resolve turbulence, it is triggered at the model boundaries using a synthetic turbulence generator (STG), which imposes spatially and temporally correlated perturbations every time-step onto the velocity components at the lateral boundaries.

Two modelling domains were connected with the one-way online nesting feature of PALM-4U (see 2.3 for more details). The initial and boundary conditions of the parent domain were taken from a WRF model simulation using the offline nesting feature of PALM-4U; the boundary conditions were updated at every model time step (2.2.2).

For more information about the PALM model, embedded modules and the PALM-4U components, see Maronga et al. (2020) and the companion papers in this special issue.

### 2.2 PALM-4U model set-up

#### 2.2.1 General model configuration

The dynamic core of the PALM-4U model was configured with the Wicker and Skamarock 5$^{th}$ order advection scheme (Wicker and Skamarock, 2002) and the multigrid pressure solver (Hackbusch, 1985; Maronga et al., 2015). The radiative fluxes were simulated by RRTMG and their interactions with the urban canopy layer were modelled by RTM (Krč et al., 2020). The surface

https://doi.org/10.5194/gmd-2020-126
Preprint. Discussion started: 4 August 2020

Geoscientific Model Development Discussions

energy balance for the individual surfaces (vegetation, pavement, buildings, water) was calculated by the LSM and BSM components (Maronga et al., 2020). The dynamic and energy processes caused by resolved trees and shrubs were modelled by PCM. The chemistry module was configured for $NO_X$, $PM_{10}$ and $PM_{2.5}$ species without chemical reactions to simulate purely the passive transport of the emitted pollutants.

#### 2.2.2 WRF model configuration

Initial and boundary conditions for the parent domain of the PALM-4U simulations were obtained from the WRF model. WRF (version 3.8.1) was run on two nested domains with horizontal resolution of 9 and 3 km, and 49 vertical levels. The dimensions of the inner domain were 187×121 grid points. The configuration was standard: NOAH LSM, RRTMG radiation and Yonsei University scheme for the planetary boundary layer (PBL). No urban parameterization has been used in the WRF model and the settings arising from the MODIS land use categories have not been altered. The WRF output data have been collected from overlapping runs of 12-hour length, initialized from the GFS operational analyses and predictions. The first six hours of each run served as a spin-up and the following hours (7–12) have been used for generation of boundary conditions for the offline nesting.

#### 2.2.3 Surface and material parameters

For solving the energy balance equations, BSM and LSM require using detailed and precise input parameters describing the surface materials (e.g., albedo, emissivity, roughness length, thermal conductivity, capacity of the skin layer, thermal capacity and volumetric thermal conductivity). Urban and land surfaces and materials become very heterogeneous in a real urban environment when going to very fine spatial resolution. Any bulk parameterization for the whole domain would be inadequate. For our study, a very detailed setting of the parameters was supplied everywhere possible. In order to obtain the data, an extensive on-site campaign was performed which provided a detailed database of geospatial data including information on wall, ground, and roof materials and colours for the estimation of surface and material properties (Resler et al., 2017). The original geo-database was extended with information about neighbouring streets and updated with new modifications (see section 2.3 for detailed description).

Surfaces are described by their respective material category, albedo, and emissivity values. Parameter estimates are assigned to categories based on surface and subsurface material composition and thickness. The parameters of all subsurface layers of the respective material were set to the same value. The skin layer parameters $C_0$ and $\Lambda$ (see Equations 1 and 2 in Resler et al., 2017) were inferred from the properties of the near-surface material, which may be different in the rest of the volume. Parameter settings of the categories used in this study are given in supplements as Table S01. Trees in the analyzed domain were described by their respective position, diameter, trunk parameters and vertically stratified leaf area density. Prague 3D model available from the Prague Institute of Planning and Development was used to obtain the building height database. Description and properties of surfaces and materials were assembled into standard GIS formats and subsequently transformed into the PALM-4U input NetCDF files corresponding to the PALM Input Data Standard (PIDS) (Heldens et al., 2020).

Geoscientific Model Development Discussions

#### 2.2.4 Model spin-up run

To initialise temperatures of walls, grounds, and roofs, a 48-hour spin-up simulation for the USM and LSM was set up. During this spin-up run, the model solves only simplified energy processes while the effects of the dynamic on the energy balance were held constant (see Maronga et al., 2020). The simplifications include e.g., a simple radiation model instead of RRTMG and switching off the window model for the window fraction of walls. The spin-up allows to establish reasonable initial temperatures inside the ground, wall, and roof material layers while keeping the computational demands within an acceptable range.

#### 2.2.5 Computational aspects

The simulation was parallelized on 480 MPI processes, 400 of them were used for the parent domain calculation and 80 for the child domain. The simulations were performed on the Salomon supercomputer of the Czech supercomputing centre IT4T and every simulation took approximately 37 hours wallclock time.

### 2.3 Study domain description

The study domain in Prague-Holešovice was adapted from Resler et al. (2017), covering the vicinity of a crossroad of Dělnická street and Komunardů street in a densely built-up area in Prague, Czech Republic (50°06.195' N, 14°27.000' E). The area is well suited for this type of study as it represents a typical Prague residential area in a rather topographically flat (terrain elevation ∼180 m a.s.l.) part of the city with a variety of urban components (old and new housing buildings, backyards, parking spaces). The two streets run north to south (Komunardů) and west to east (Dělnická), and have the width of roughly 25 and 17 m, respectively. The buildings in the area range approximately from 10 to 35 m in height. There is not much vegetation in the area and the majority of the trees is located in the courtyards. The surrounding neighbourhood is very similar to the study area (Fig. 1).

A few minor modifications were made to the study domain from the previous analysis of Resler et al. (2017). Firstly, the horizontal extent of the domain was extended from the original 376 m × 226 m to 400 m × 256 m. This was important for the domain multiplication in a synthetic domain setup (see section 2.4); the new domain ends in the middle of streets in all directions. Secondly, the central part of the intersection, where a small asphalt polygon (∼11 m$^2$) in the real street was partially replaced by cobblestones (∼7 m$^2$ of cobblestones and ∼4 m$^2$ of asphalt), was modified in the input data accordingly. Last minor change from the previous analysis is the height of the highest building which was physically rebuilt and is now 35 m high. The domain covers the area of 102,400 m$^2$, of which 48,356 m$^2$ is the total building footprint, 48,356 m$^2$ (∼22.9% of total domain surface area) are impervious or anthropogenic surfaces and 5,593 m$^2$ (∼2.7%) are pervious surfaces (e.g., grass). Each building has three levels – lower, often markets and shops; upper, typically residential; and roof. Lower level is covered by 9,933 m$^2$ (∼4.7%) of windows and 20,837 m$^2$ (∼9.9%) of walls, upper level is covered by 22,861 m$^2$ (∼10.8%) of windows and 52,169 m$^2$ (∼24.7%) of walls. Roof area is 51,044 m$^2$ (∼24.2%). Total area of all surfaces in the domain is 210,793 m$^2$. In the time of this study, 158 trees are planted in the area of which 4 are coniferous and 154 are broad-leaved.

https://doi.org/10.5194/gmd-2020-126
Preprint. Discussion started: 4 August 2020


Geoscientific Model Development
Discussions

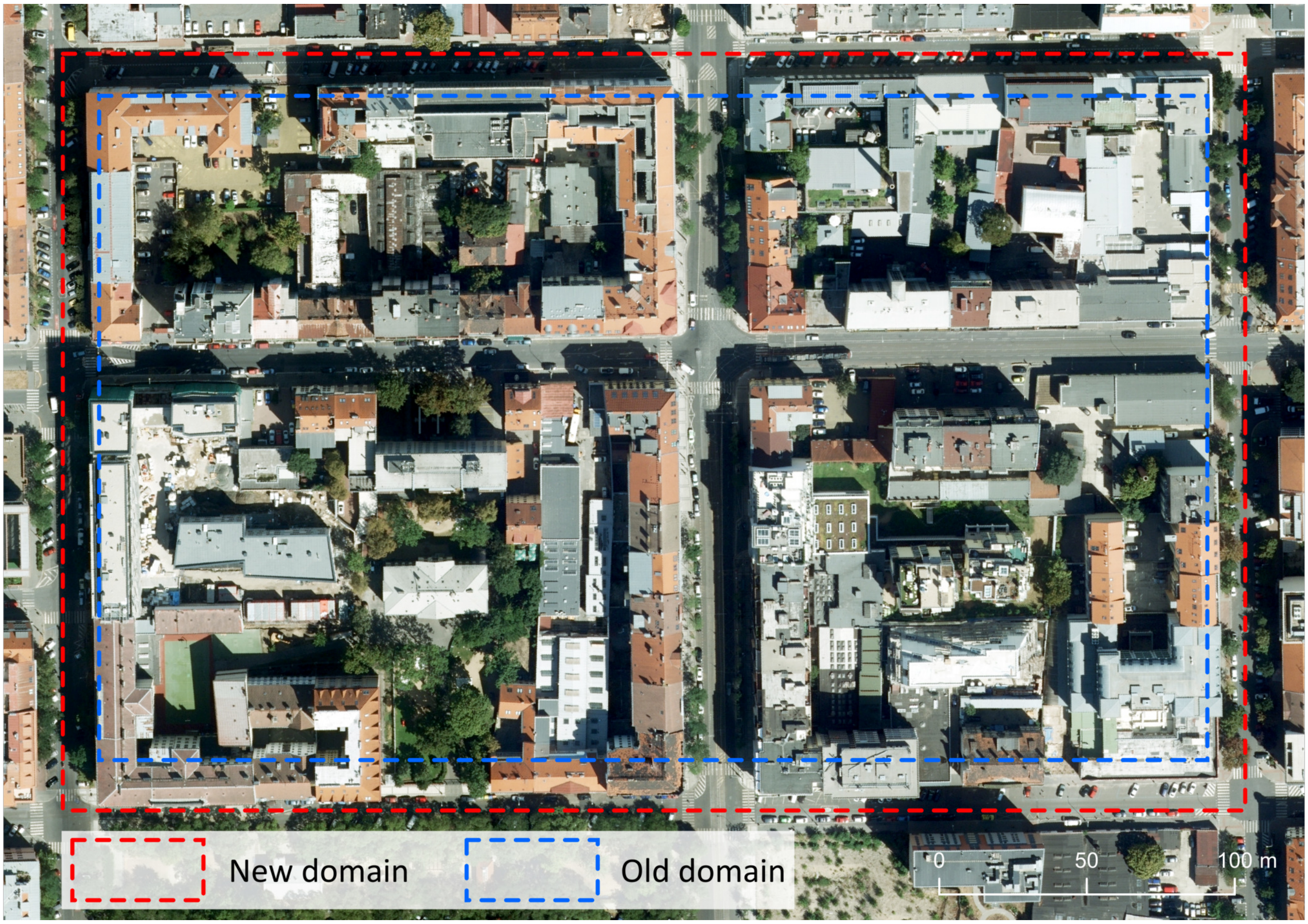


**Figure 1.** Domain in Prague-Holešovice with the old (blue) and new (red) extended domain (EPSG: 32633, orthophoto source: Institute of Prague Development)

### 2.4 Synthetic modelling domains

The study domain described above is too small for realistic large-eddy simulations, because the largest turbulent eddies are of size of the boundary layer height, which can reach up to 2–3 km in summertime. In order to resolve the turbulent transport of these eddies, the horizontal model domain size must be at least 2–3 times the boundary layer height and thus be in the order of several square kilometres, which is much larger than the employed model domain in the present study (Resler et al., 2017). Moreover, to allow simulations of real meteorological conditions, non-cyclic boundary conditions with offline nesting were considered, using the meteorological model WRF and a synthetic turbulence generator. This setting, however, requires a sufficient horizontal extent of the domain to allow development of the correct turbulent flow. For this purpose, a nested two

https://doi.org/10.5194/gmd-2020-126
Preprint. Discussion started: 4 August 2020

Geoscientific Model Development Discussions

domain setup with one-way online nesting was utilized as described in section 2.1 and synthetic domains were generated by horizontal multiplying of the original domain.

The parent domain had a horizontal grid spacing of 8 m and was created by seven repetitions of the original domain in west-east direction and eleven repetitions in south-north direction. Moreover, an additional flat buffer zone was added on all sides of the domain. The width of this buffer was 25 grid cells at the west and east boundaries and 24 grid cells at the south and north boundaries. Thus, the extent of the complete parent domain is 400×400 grid cells (3200 m × 3200 m) in both directions. The domain was configured with 120 vertical layers using the layer stretching approach so that the vertical grid spacing of 8 m was stretched above 120 m by a factor of 1.08 until a grid spacing of 24 m was reached. The resulting domain top was at 2.5 km.

The nested fine resolution domain (hereafter child domain) was configured with a refinement ratio of 4, having a 2m grid resolution in all directions and it consisted of four original domains; two in west-east direction and two in south-north direction. The extent of the domain was 400×256×40 grid cells (800 m × 512 m × 80 m). The child domain was located asymmetrically in the left part of the parent domain and the evaluation was done on the south-west part of it (see Fig. 2). This configuration was selected due to east wind flow during the modelled episode.

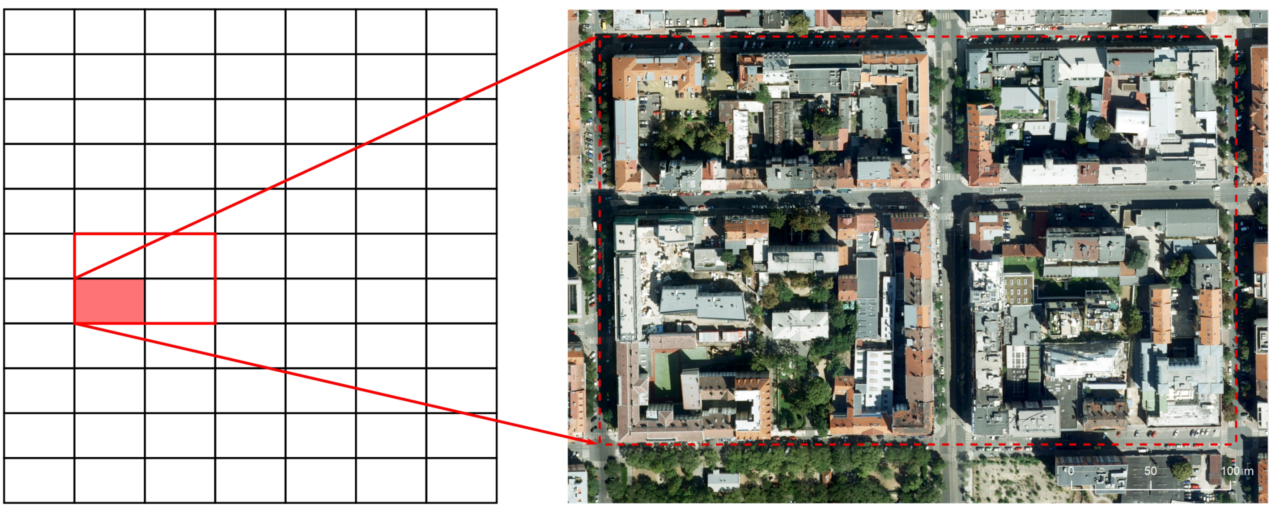

**Figure 2.** Design of model domains; black-bordered rectangles representing the parent domain, red-bordered rectangle representing the child domain. Solid red rectangle represents one unique domain with the real environment before multiplication. EPSG: 32633, orthophoto source: Institute of Prague Development.

https://doi.org/10.5194/gmd-2020-126
Preprint. Discussion started: 4 August 2020

Geoscientific Model Development
Discussions

### 2.5 The modelled heatwave episode

This study focuses on modelling the thermal comfort and therefore a heatwave episode on 2–3 July 2015 was chosen for these simulations. One advantage of this choice is that the previous version of the model was also validated on this period (see Resler et al., 2017). A detailed description of the weather during the modelled period is also provided in Resler et al. (2017). The weather was characterized by a high-pressure system centred above the Baltic Sea with mostly clear skies and the daily maximum temperature exceeding 30 °C while the minimum not falling below 20 °C (tropical night). Relative humidity values ranged from 30% during the day to 65% at night. Easterly winds were observed with values mostly below 2.5 $m.s^{-1}$ above the roof level. Maximum wind speed of 3–4 $m.s^{-1}$ in 10 m height was observed at the Karlov station (WMO 11519) in the afternoon of 2 July 2015, during the spin-up, and at the end of 3 July 2015. At night, a south/south-east low-level jet was observed in the atmospheric soundings, with a 10 $m.s^{-1}$ maximum wind speed at 640 m a.s.l. (950 hPa). The time of the sunset was 19:15 UTC on 2 July 2015, sunrise at 2:58 UTC and solar noon at 11:06 UTC on 3 July 2015.

### 2.6 Air pollution and emissions

Air pollution sources for our case are dominated by the local road traffic. The emission flux is estimated based on the daily traffic intensities, which are available from annual traffic census data, for all streets in both directions. Emission factors (taken from local Czech database; MEFA, 2013) give pollutant release per vehicle per meter of travel, based on vehicle and fuel type. For our study area, the assumption was that all vehicles are passenger cars, which is reasonable for this residential neighbourhood. The pollutant of interest is $PM_{10}$. The traffic-related $PM_{10}$ emissions are spatially uniformly distributed into traffic lanes and temporally distributed using prescribed hourly factors also derived from available annual traffic census data (see Fig. 3 for daily spatial distribution).

### 2.7 Sensitivity tests

For the evaluation of the influence of the parameter changes, a *baseline* simulation was performed in which the parameters tested were set to real values. The scenario simulations then changed one or more of these parameters.

#### 2.7.1 Synthetic scenarios - sensitivity to the setting of material parameters

For the first group of sensitivity tests, a suite of basic scenarios was selected based on the most important variables in the street environment. These scenarios target potential biases in the model outputs connected to the erroneous setting of material and building input parameters such as albedo or roughness. These parameters are notoriously difficult to obtain with a sufficient resolution and are thus usually set in a very general way and sometimes even tuned to the model results. As model errors can stem from many different sources (e.g., model deficiencies, chaotic behavior, imperfect input data), we aim to quantify which part of the error can be attributed to the setting of these parameters.

Some parameters used were already validated in the previous paper by Resler et al. (2017), but since the PALM modelling system has been extended with new features after 2017, an update was necessary for new parameters. According to the new


**Figure 3.** $PM_{10}$ emitted by the cars along their trajectories in Prague-Holešovice. Concentrations were summarized in g.day.m$^{-2}$ and disaggregated to 1-hour time steps. EPSG: 32633, orthophoto source: Institute of Prague Development.

functionalities, window and wall fractions were mapped for each building in USM and more detailed plant canopy parameters were included in PCM. In total 21 basic scenarios were prepared that each changes one specific parameter of the surfaces (and/or plant canopy) from the baseline simulation (hereafter "SA" scenarios). Table 1 summarizes the parameter changes for the SA scenarios, the surfaces affected by the change and the fraction of the total surface area affected in the respective scenario.

### 2.7.2 Real-life scenarios - sensitivity to urban heat island mitigation measures

The second group of scenarios was designed more from the urban planners' point of view, i.e., assessing the influence of (in)appropriate urban planning actions to improve thermal comfort and air quality. These scenarios present several measures

https://doi.org/10.5194/gmd-2020-126
Preprint. Discussion started: 4 August 2020

Geoscientific Model Development Discussions
Open Access
EGU

**Table 1.** Scenarios testing model sensitivity to changes of material parameters with fraction of affected domain surface area (column Surf. fraction). Detailed description of surfaces is in section 2.3.

| **Scenario** | **Description** | **Surfaces** | **Surf. fraction (%)** |
|---|---|---|---|
| SA01 | Albedo increase +20% | Walls, roofs, surfaces | 100.0 |
| SA02 | Albedo decrease -20% | Walls, roofs, surfaces | 100.0 |
| SA03 | Emissivity set to the average for each group of surfaces | Land cover: 0.8922; Lower walls: 0.9263; Upper walls: 0.9278; Roofs: 0.7233 | 100.0 |
| SA04 | Average SA03 emissivity +20% | Average = SA03, max. 1.0 | 100.0 |
| SA05 | Average SA03 emissivity -20% | Average = SA03 | 100.0 |
| SA06 | Roughness increase +20% | Walls, roofs, surfaces | 100.0 |
| SA07 | Roughness decrease -20% | Walls, roofs, surfaces | 100.0 |
| SA08 | Thickness increase +20% | Walls, roofs, surfaces | 100.0 |
| SA09 | Thickness decrease -20% | Walls, roofs, surfaces | 100.0 |
| SA10 | Transmissivity of windows increase +20% | Walls (windows only) | 15.6 |
| SA11 | Transmissivity of windows decrease -20% | Walls (windows only) | 15.6 |
| SA12 | Thermal conductivity inside of wall increase +20% | Walls | 34.6 |
| SA13 | Thermal conductivity inside of wall decrease -20% | Walls | 34.6 |
| SA14 | Volumetric heat capacity increase +20% | Walls, roofs, surfaces | 100.0 |
| SA15 | Volumetric heat capacity decrease -20% | Walls, roofs, surfaces | 100.0 |
| SA16 | Window fraction increase +20% | Walls | 18.7 |
| SA17 | Window fraction decrease -20% | Walls | 12.5 |
| SA18 | Leaf area density increase +20% | Trees | |
| SA19 | Leaf area density decrease -20% | Trees | |
| SA20 | Soil moisture increase +20% | Pervious surfaces only | 2.7 |
| SA21 | Soil moisture decrease -20% | Pervious surfaces only | 2.7 |

https://doi.org/10.5194/gmd-2020-126
Preprint. Discussion started: 4 August 2020



**Table 2.** Scenarios testing sensitivity of the model results to UHI mitigation measures

| **Scenario** | **Description** | **Note** |
|---|---|---|
| SB01 | Building height increase +20% | Street canyon ratio |
| SB02 | Building height decrease -20% | Street canyon ratio |
| SB03 | All surfaces (pavement) changed to asphalt | Land cover |
| SB04 | All surfaces (pavement) changed to concrete | Land cover |
| SB05 | All surfaces (pavement) changed to cobblestones | Land cover |
| SB06 | All surfaces (pavement) changed to white cobblestones | Land cover |
| SB07 | Tram green line | Land cover |
| *SB08** | *All surfaces insulated* | *Walls only* |
| SB09 | Water channel instead of tram line, roads were changed to grass | Land cover, no changes in emissions |
| SB10 | Green areas changed to asphalt, trees were deleted | Grey city 1 |
| SB11 | Asphalt except main roads and pavements changed to grass, all trees deleted | Grey city 2 |
| SB12 | Planted trees on each possible place; placed 128 acer platanoides | Green city |
| SB13 | New tree alley: Delnicka, center-line position | Acer platanoides |
| SB14 | New tree alley: Delnicka, both-side position | Acer platanoides |
| SB15 | New tree alley: both streets, both-side position | Acer platanoides |
| SB16 | All trees coniferous | More dense crown |
| SB17 | Include anthropogenic heat flux | A/Cs, heating etc. |

* Scenario SB08 was removed from further analysis, because results were significantly affected by numerical instability solved in PALM SVN revision 4240.

typically taken into account when dealing with the UHI effect, such as greening or changes in the surface materials. Detailed description of this group of scenarios (hereafter denoted by the "SB" prefix) is included in Table 2.

## 3 Results

Due to a different nature of the two sets of scenarios, the analysis of the model results will be performed separately for the more synthetic SA scenarios and real-life SB scenarios. However, some aspects of the analysis are common for both. Chaotic nature of the turbulent flow in the domain requires an application of time averaging which needs to be sufficiently long to smooth out turbulent fluctuations, yet short enough to capture the diurnal variability. In the time series plots, we opted to show 10-minute averaged values together with hourly moving averages. Summary tables, on the other hand, show three-hour averages along with daily averages, minima and maxima. One important aspect of the modelling setup which must be kept in mind when analyzing the results is that the model spin-up period uses a constant dynamic and simplified energy model (see section 2.2.4) and thus the initial thermal conditions (grounds, walls, and roofs temperatures) are not in total agreement with temperatures obtained by a full model run. This can impose differences of the simulation behaviour in the first hours from standard behaviour in the following hours when this initial effect vanishes which may limit the applicability of the results in the first few hours of the simulation.

Spatial variability is analysed by averaging over the whole domain as well as separately over several selected domain parts. A particular focus is on the two crossing streets and courtyards. For maps with point positions and area selections see the supplemental material (SFig01-09). The most important variables for the end users were chosen as primary indicators. They include air temperature, surface temperature, $PM_{10}$ concentrations and two biophysical temperature characteristics (MRT – mean radiant temperature and PET – physiological equivalent temperature) all in the height of the human body represented by the first 2m high layer. Where necessary, additional variables of the energy balance were analyzed.

All scenario simulations are analyzed with respect to the baseline simulation, which is simply a model run with the original parameter values from the data sources. Fig. 4 shows spatial distribution of basic variables in the domain for the baseline simulation.

### 3.1 Sensitivity to material parameters

In the first part of the assessment, we analyze the model sensitivity to the setting of building and material parameters such as albedo or roughness (SA scenarios). Table 3 summarizes differences of each SA scenario from the baseline in air temperature for the whole domain as an example. Differences for other variables and absolute values are summarized in Table S02 in supplementary files. Results are averaged for several areas: domain, east-west street (Dělnická), south-north street (Komunardů), both streets (Streets) and courtyards (see supplement for area and point locations and Table S02 summarizing results over the whole domain and for other variables).

In general, the following four parameters show the highest sensitivity in temperature in the following settings: albedo (SA01, SA02), emissivity (SA03–05), thermal conductivity of walls (SA12, SA13) and volumetric heat capacity (SA14, SA15) with average response up to $\pm 0.1$ K and maximum response reaching up to $\pm 0.18$ K in three-hour averages and up to $\pm 0.4$ K in 10-minute averages for some parameters during the day. Overall, the albedo setting (SA01, SA02) shows the highest sensitivity of all parameters in this group. The lowest sensitivity is observed for wall thickness (SA08, SA09), transmissivity of windows (SA10, SA11) and soil moisture (SA20, SA21). However, the reason for the low sensitivity to the changes of the soil moisture lies mainly in a low percentage of the green areas in the domain. Small areas covered with or in direct vicinity of vegetation are influenced significantly (Fig. 5).

The daily cycle of air temperature also has an imprint in the relative importance of respective parameters throughout the day. Parameters used in incoming radiation routines (namely albedo; SA01, SA02) are the most sensitive ones in the middle of the day, when the radiative balance is governed mostly by incoming shortwave radiation. During the night, emissivity (SA03–05) and heat capacity of walls (SA14, SA15) play a major role (see Table 3), thus sensitivity to these parameters is higher then. Some parameters show quite high sensitivity only in short periods during the day. For example window fraction shows low

https://doi.org/10.5194/gmd-2020-126
Preprint. Discussion started: 4 August 2020


Geoscientific Model Development
Discussions

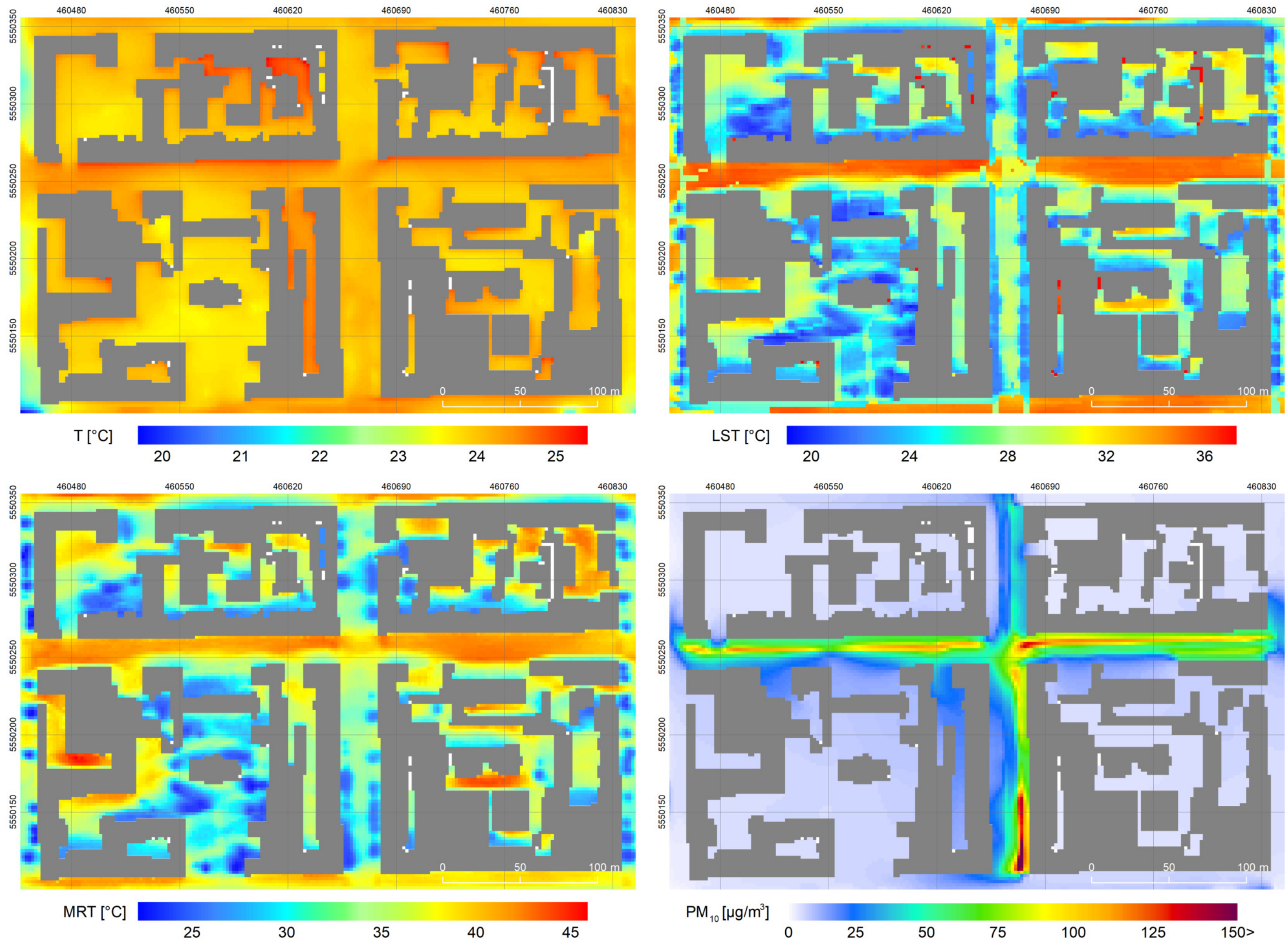


**Figure 4.** Daily average spatial variability of air temperature (top left), surface temperature (top right), mean radiant temperature – MRT (bottom left) and $PM_{10}$ concentrations (bottom right) for the baseline simulation. EPSG: 32633, layer with roofs is own data source.

sensitivity in the morning hours, after which it increases around 9–12 UTC (11–14 local time) and peaks in the early evening around 18–21 UTC (see SA16–17 in Table 3).

Air temperature, though fundamental for physical evaluation, is not necessarily the best quantity for evaluating biophysical properties, namely thermal comfort. For this purpose, variables combining other relevant physical variables (radiation, humidity, air flow, etc) are used. Two common examples are the mean radiant temperature (MRT) and physiological equivalent temperature (PET) which we use in this analysis. Given the combination of various influences, MRT and PET often show opposite behaviour to the air temperature in terms of the sign of the changes with higher absolute values. As a demonstration we show this on the two most prominent scenarios SA01 and SA02. In SA01, the albedo is increased by 20%, which results in the decrease of daily surface temperatures by 0.5 K and a decrease of around 0.1 K for air temperature. On the other hand, by

https://doi.org/10.5194/gmd-2020-126
Preprint. Discussion started: 4 August 2020



**Table 3.** Differences in air temperature in the model first layer in K over the whole domain for SA scenarios (Scen): 24-hour (AVG) and 3-hour averages (00–03 to 21–24), minimum (MIN), maximum (MAX) and times (TIME).

| Scen | AVG | 00–03 | 03–06 | 06–09 | 09–12 | 12–15 | 15–18 | 18–21 | 21–24 | MIN | TIME | MAX | TIME |
|---|---|---|---|---|---|---|---|---|---|---|---|---|---|
| SA01 | -0.111 | -0.039 | -0.087 | -0.135 | -0.143 | -0.161 | -0.137 | -0.113 | -0.071 | -0.374 | 12:20 | 0.032 | 12:30 |
| SA02 | 0.098 | 0.036 | 0.066 | 0.117 | 0.159 | 0.143 | 0.120 | 0.085 | 0.060 | -0.066 | 11:40 | 0.349 | 12:10 |
| SA03 | 0.000 | -0.002 | 0.011 | -0.012 | 0.018 | -0.020 | -0.004 | -0.002 | 0.009 | -0.126 | 08:00 | 0.110 | 09:30 |
| SA04 | -0.055 | -0.069 | -0.068 | -0.041 | -0.063 | -0.030 | -0.038 | -0.066 | -0.062 | -0.171 | 10:30 | 0.063 | 06:50 |
| SA05 | 0.095 | 0.118 | 0.129 | 0.066 | 0.062 | 0.062 | 0.074 | 0.121 | 0.125 | -0.081 | 13:20 | 0.264 | 11:20 |
| SA06 | 0.014 | 0.054 | 0.049 | 0.024 | 0.038 | 0.005 | -0.020 | -0.035 | -0.005 | -0.090 | 10:10 | 0.148 | 09:30 |
| SA07 | -0.033 | -0.093 | -0.087 | -0.090 | -0.054 | -0.010 | 0.017 | 0.035 | 0.014 | -0.176 | 06:20 | 0.101 | 13:30 |
| SA08 | 0.005 | 0.002 | -0.005 | 0.004 | 0.022 | 0.015 | -0.005 | 0.000 | 0.002 | -0.100 | 13:10 | 0.139 | 14:50 |
| SA09 | 0.000 | -0.002 | -0.008 | -0.005 | 0.015 | -0.009 | 0.010 | 0.001 | 0.001 | -0.131 | 13:50 | 0.166 | 12:00 |
| SA10 | -0.001 | 0.000 | -0.005 | 0.001 | 0.005 | -0.004 | -0.004 | -0.004 | 0.004 | -0.161 | 10:10 | 0.141 | 08:40 |
| SA11 | 0.002 | 0.001 | 0.007 | -0.010 | 0.017 | -0.003 | -0.001 | 0.003 | 0.002 | -0.124 | 10:30 | 0.087 | 13:30 |
| SA12 | -0.020 | 0.050 | 0.035 | -0.067 | -0.093 | -0.075 | -0.046 | 0.002 | 0.034 | -0.248 | 10:50 | 0.162 | 12:30 |
| SA13 | 0.001 | -0.092 | -0.069 | 0.051 | 0.072 | 0.060 | 0.043 | -0.007 | -0.053 | -0.127 | 02:50 | 0.206 | 10:00 |
| SA14 | 0.015 | 0.097 | 0.085 | -0.024 | -0.053 | -0.060 | -0.018 | 0.026 | 0.065 | -0.202 | 13:50 | 0.137 | 02:20 |
| SA15 | -0.026 | -0.141 | -0.121 | 0.025 | 0.071 | 0.047 | 0.020 | -0.034 | -0.076 | -0.189 | 02:50 | 0.130 | 11:50 |
| SA16 | -0.036 | -0.037 | -0.018 | -0.004 | -0.019 | -0.044 | -0.036 | -0.077 | -0.049 | -0.119 | 10:30 | 0.080 | 10:00 |
| SA17 | 0.028 | 0.035 | 0.000 | -0.008 | 0.025 | 0.001 | 0.051 | 0.070 | 0.053 | -0.146 | 13:10 | 0.105 | 13:30 |
| SA18 | -0.016 | -0.005 | -0.012 | -0.010 | -0.023 | -0.032 | -0.029 | -0.013 | -0.003 | -0.151 | 10:10 | 0.162 | 10:00 |
| SA19 | 0.018 | -0.007 | 0.010 | 0.010 | 0.042 | 0.034 | 0.039 | 0.015 | 0.006 | -0.087 | 10:30 | 0.145 | 11:30 |
| SA20 | -0.008 | -0.008 | -0.007 | -0.018 | -0.010 | -0.016 | 0.001 | -0.006 | -0.003 | -0.206 | 10:10 | 0.107 | 10:20 |
| SA21 | 0.008 | 0.005 | -0.001 | 0.014 | 0.016 | -0.005 | 0.021 | 0.007 | 0.011 | -0.135 | 10:30 | 0.128 | 10:00 |

increasing reflection at the surfaces, this change increases both MRT and PET by 0.6 K and 0.3 K respectively. In daily maxima, the increase of both biometeorological variables is even more prominent and reaches up to 1.7 K and 1.6 K respectively. Decreasing albedo by 20% in SA02 has a similar effect in absolute numbers with the opposite sign.

Influence on air quality, represented here by changes of $PM_{10}$ concentrations in the first layer, originating from emission from local transportation, is much less significant. For the dominant parameters, such as albedo or emissivity, we still observe a similar general tendency to increase (decrease) $PM_{10}$ values with increased (decreased) albedo (emissivity). This behaviour is opposite to the surface and air temperatures and it is likely primarily caused by connected changes in the flow regime as illustrated in Fig. 6 and 7 by decrease (increase) of wind speed with increased (decreased) albedo (also discussed in e.g. Žák et al., 2016). Long-term average changes are generally small and with the exception of a singular peak (Fig. 8) lying within $\pm 5\%$ in most of the domain.

https://doi.org/10.5194/gmd-2020-126
Preprint. Discussion started: 4 August 2020

Geoscientific Model Development
Discussions
Open Access

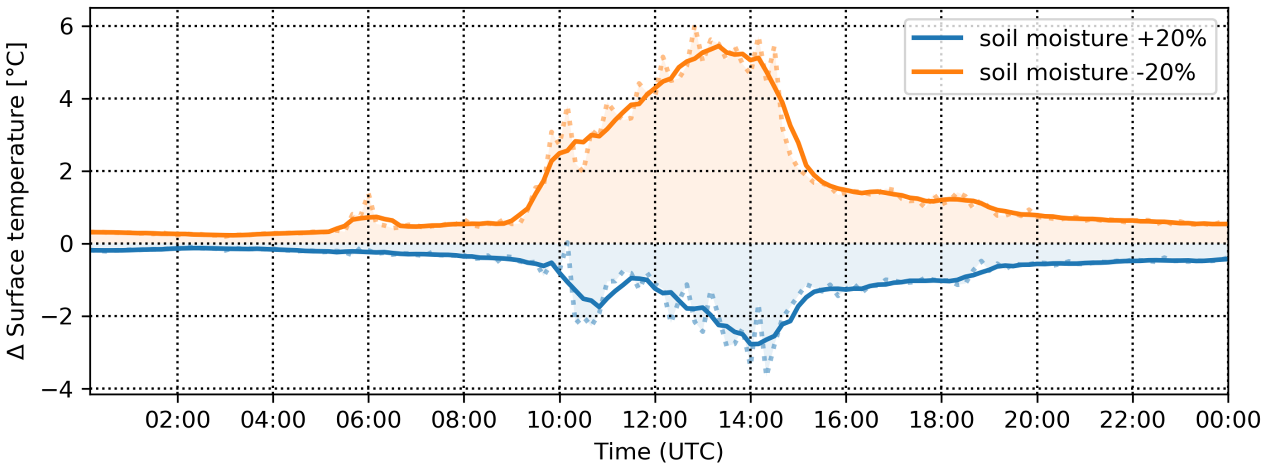


**Figure 5.** Soil moisture sensitivity of surface temperature difference for scenario SA20 (blue line) and SA21 (orange line) at point F03.

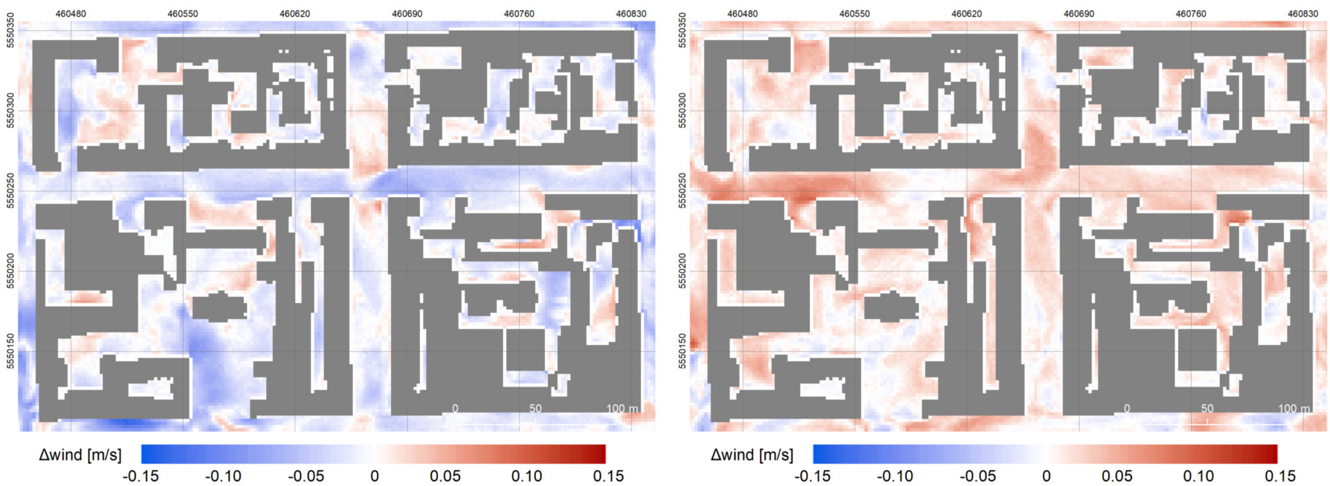


**Figure 6.** Daily average sensitivity of horizontal wind speed (1m) expressed as the difference between scenario and baseline. Left: scenario SA01 (albedo increased by 20%); right: scenario SA02 (albedo decreased by 20%). EPSG: 32633, layer with roofs is own data source.

https://doi.org/10.5194/gmd-2020-126
Preprint. Discussion started: 4 August 2020




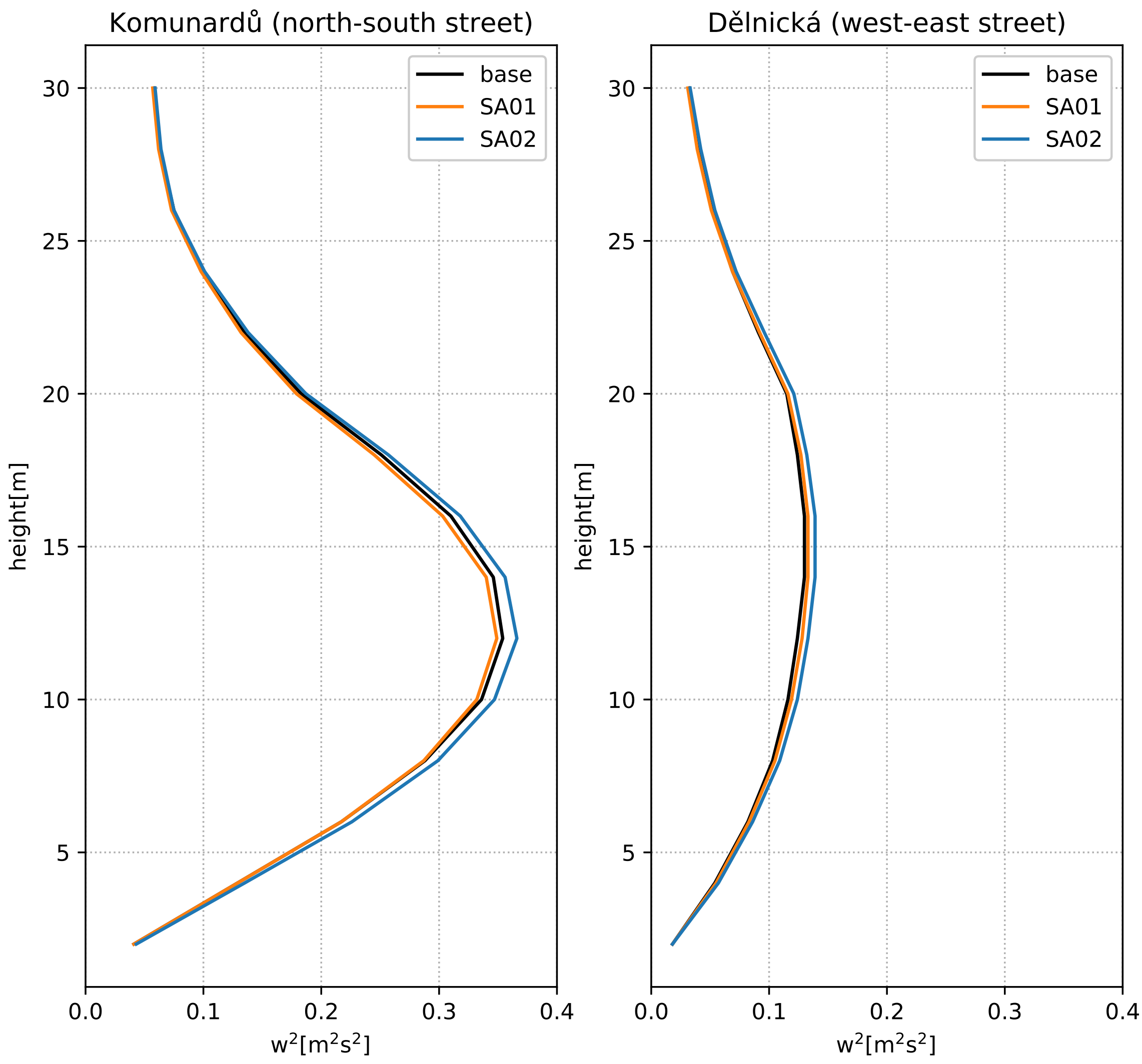


**Figure 7.** Daily average profiles of $w^2$ averaged over the two main streets: the north-south oriented Komunardů (left) and the west-east oriented Dělnická (right).

https://doi.org/10.5194/gmd-2020-126
Preprint. Discussion started: 4 August 2020




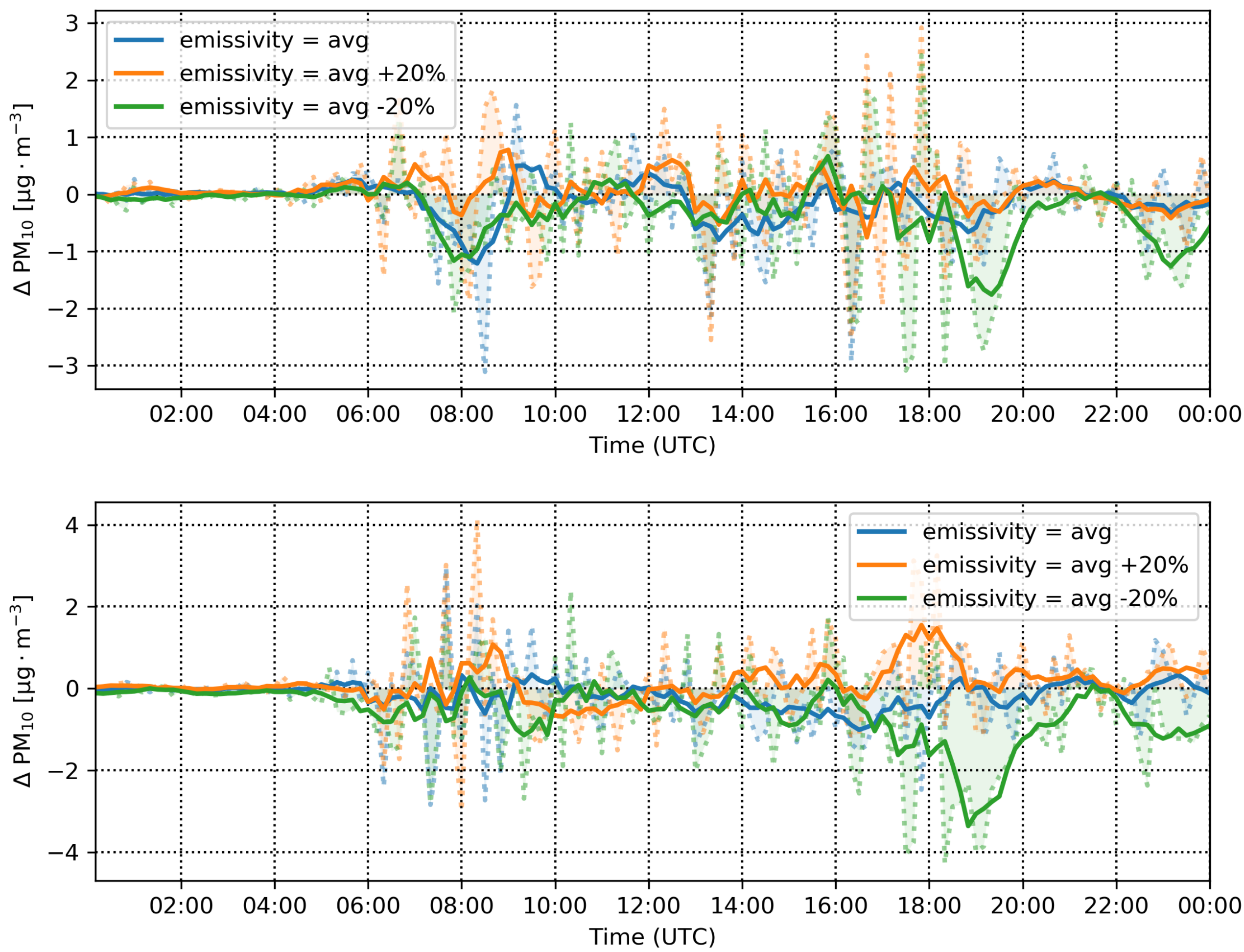


**Figure 8.** Emissivity scenario for north-west courtyard (top) and domain average (bottom) for scenarios SA03 (blue), SA04 (orange) and SA05 (green)

https://doi.org/10.5194/gmd-2020-126
Preprint. Discussion started: 4 August 2020

Geoscientific Model Development
Discussions

The parameters we analyse influence the results mainly by changing the energy balance of the horizontal and vertical surfaces in the model domain. Air temperature changes are then mainly driven by the transfer of heat between these surfaces and air. In this context, we will now focus on the effect on surface temperatures. The highest sensitivity of surface temperature is observed in the same scenarios as for air temperature; albedo SA01, SA02 (Fig. 9 and 10), emissivity SA03–05, thermal conductivity SA12, SA13 and volumetric heat capacity SA14, SA15. The average response reaches up to ±0.5 K and the 3-hour maxima up to ±0.9 K with albedo changes (SA01, SA02) and decreased emissivity (SA05).

The model response to the surface parameters is also dependent on the location. This stems mainly from the differences in the radiation budget during the day caused by positioning of urban elements (buildings and trees). At individual points, the differences of surface temperature with respect to the base case reach up to ±4 K in shorter periods in the albedo change scenarios SA01 and SA02 (e.g., points C02, C05, D05; Fig. 9).

In some parts of the domain, the typical daily cycle of the differences is even reversed in certain periods of the day. A typical example of this behaviour is the sensitivity of surface temperature to albedo changes (Fig. 9 and 10). While most surfaces show an expected increase (decrease) of temperature with the decrease (increase) of albedo, some analysis points (eg. A02, A04, B04, B06, D13, D14) show reverse influence. In other words, higher (lower) albedo results in higher (lower) surface temperatures in some parts of the day, when presumably increased (decreased) reflection from other surfaces brings more (less) SW radiation at these points compared to the base case (Fig. 11).

### 3.2 Sensitivity to urban heat island mitigation measures

The second part of the sensitivity analysis focuses on the real-life scenarios. These scenarios include UHI mitigation measures, which planners and decision makers might apply to improve the bioclimatic situation in the city during high temperature conditions, especially heatwaves. Typically considered measures include planting trees or changing surface materials (Table S02). As a contrast to SA scenarios, SB scenarios usually require changing more than one parameter at once. For instance, replacing concrete with grass results in changes in albedo, emissivity, roughness as well as other parameters.

Sensitivity of the air temperature to SB scenarios is summarized in Table 4. The changes in other variables are shown in Table S02 in the supplementary material.

The most significant changes are observed in scenarios SB09 (land cover changes), SB10 (green city 1), SB11 (green city 2), while for air temperatures, SB09–11, SB12 (green city with many planted trees), SB14 (new tree alley with both-side position on Delnicka street) and SB15 (new tree alley with both-side position on both streets) show the strongest sensitivity. Scenario SB09, in which grass replaces roads and a tram line is replaced with a water channel, shows a decrease of surface temperatures by up to 3.0 K and up to 0.3 K for air temperature. Grey city scenarios SB10 and SB11 (Fig. 12), on the other hand, tend to increase temperatures significantly with 3-hour maximum differences exceeding 2 K on the horizontal surfaces, whereas for air temperatures an increase by 0.3 K and 0.1 K, respectively, is found. However, this difference between the two scenarios is dependent on the area of interest. For example, in the north-south street (Komunardů), the change in air temperatures is much more consistent between the scenarios with maxima reaching +0.5 K in the late afternoon (Table S02 in supplement).

https://doi.org/10.5194/gmd-2020-126
Preprint. Discussion started: 4 August 2020

Geoscientific Model Development
Discussions

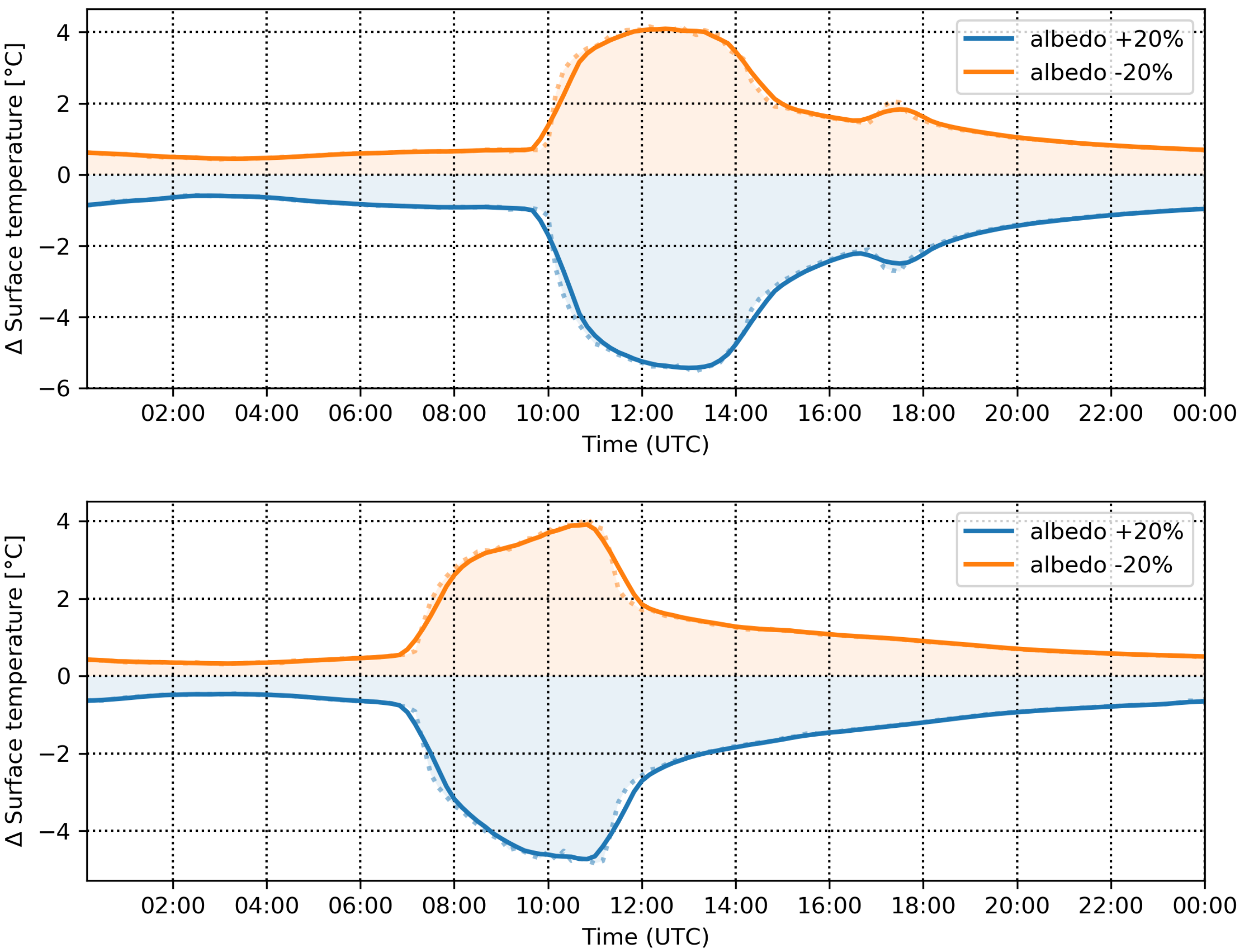


**Figure 9.** Differences in surface temperature in point C02 (top) and C05 (bottom) for scenarios SA01 (blue) and SA02 (orange)

Scenario SB12 (green city with many planted trees) appears the most effective in decreasing temperature during the day with surface temperature cooler by up to 4.0 K and air temperature by almost 0.5 K (Fig. 13). The effect is smaller during the nighttime, when the decrease in temperature is 0.8 K and 0.12 K, respectively. Instead, scenario SB09 and even SB11 (removing trees but increasing grass covered area) show decreases of more than 1.0 K and 0.15 K in the surface and air temperatures.

In terms of thermal comfort, the two analyzed characteristics (MRT and PET) show a behaviour qualitatively similar to the physical temperatures. Again, the SB12 scenario (green city with many planted trees) shows the most effective reduction with maximum decrease around 9 K in MRT and 4 K in PET in the entire domain. However, the effect varies considerably in space. The strongest change is observed in the west-east oriented Dělnická street while the north-south oriented Komunardů street shows a much smaller decrease of 0.0–1.2 K (Fig. 14). This difference can be partly attributed to the geometric orientation of

https://doi.org/10.5194/gmd-2020-126
Preprint. Discussion started: 4 August 2020

Geoscientific Model Development
Discussions

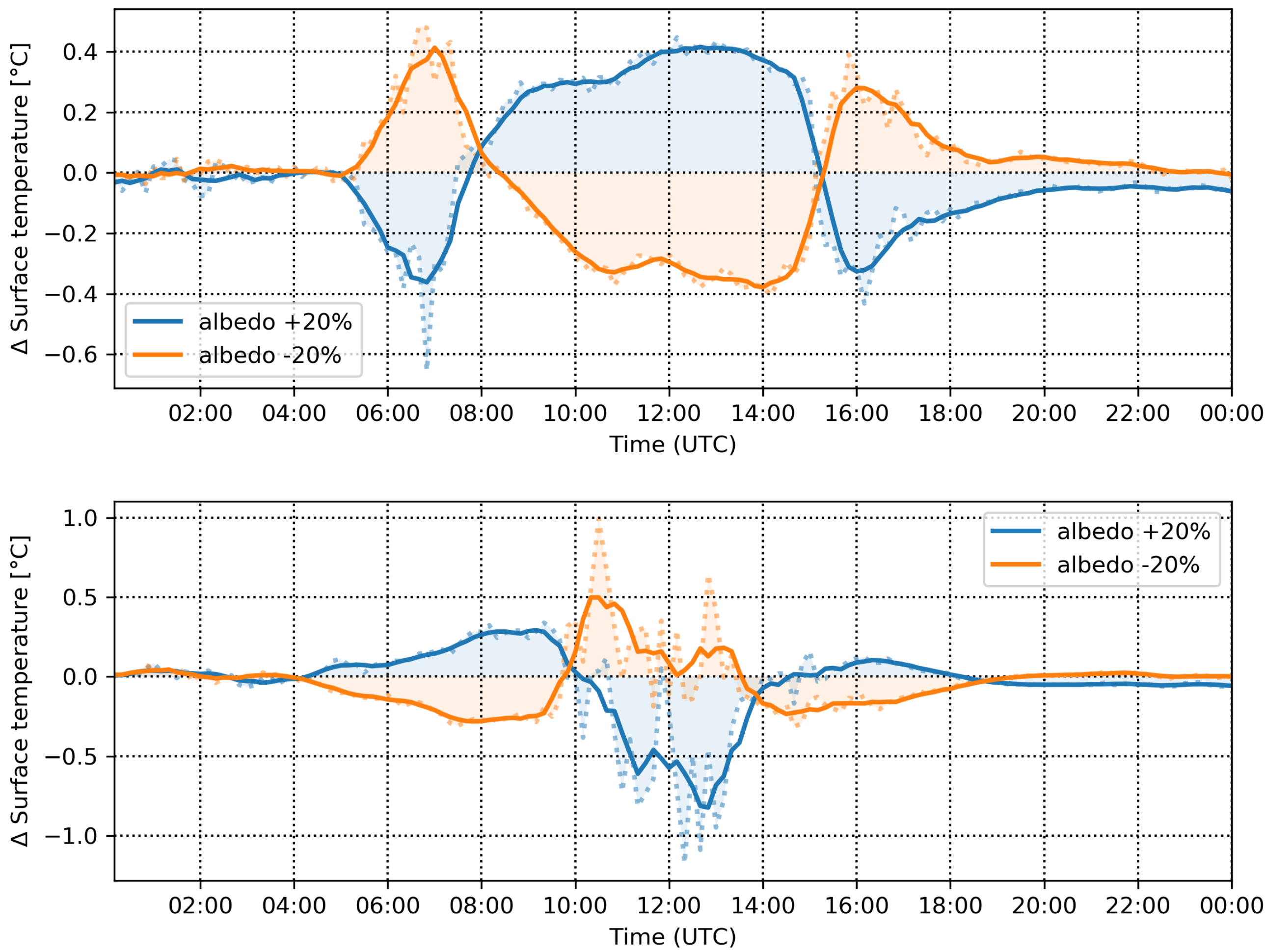


**Figure 10.** Differences in surface temperature in point A02 (top) and D14 (bottom) for scenarios SA01 (blue) and SA02 (orange)

the streets and consequent differences of insolation during the day, but also to the actual number of trees added with respect to the base case, in which more trees already grow in Komunardů st. Similar behaviour is shown in SB13–SB15 scenarios (new tree alley/-s scenarios) with decreases up to 4.0 K in MRT and 1.6 K in PET on average.

On the other hand, SB10 and SB11 scenarios (grey city 1 and 2) show a significant increase of both biophysical properties. The MRT is increased by 8 K (5 K) and PET by 3 K (1.6 K; see Fig. 15) around noon in the entire domain in SB10 (SB11). Similarly to the previous comparison, there is a marked spatial difference throughout the domain. However, the effect is strongest in the Komunardů street, with an increase of over 12 K (MRT) and 3 K (PET), and courtyards (over 9 K/4 K), while in the Dělnická street, the increase is only around 3 K in MRT and 1 K in PET.

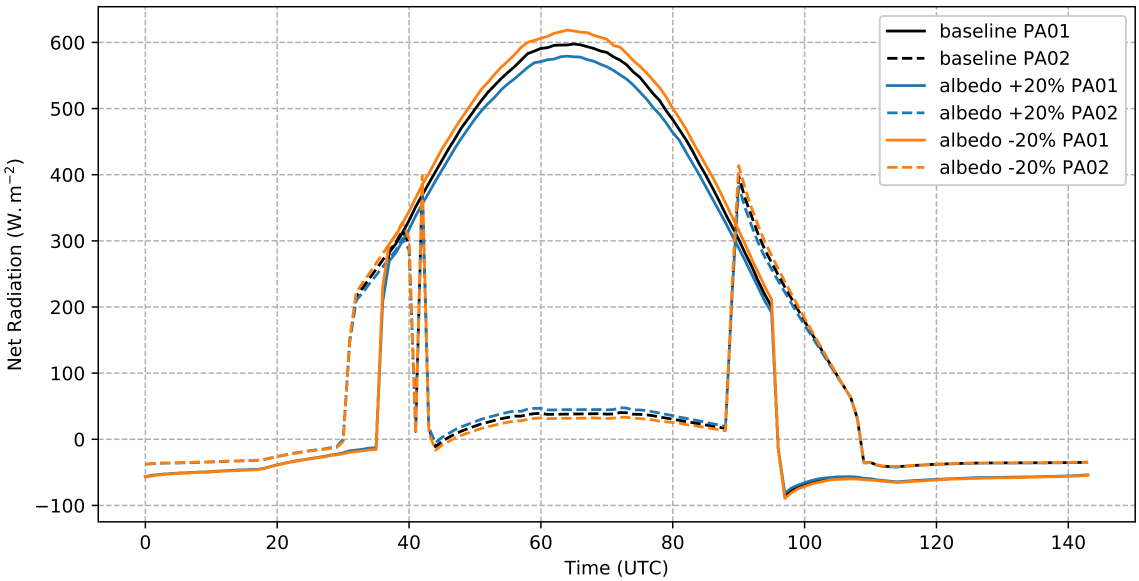


**Figure 11.** Net radiation at points A01 and A02 in scenarios with increased/decreased albedo compared to the baseline.

Unlike for the sensitivity cases SA, $PM_{10}$ shows a significant dependence on the measures applied. However, the influence is almost universally inverse to the one for temperature. Generally, decreasing surface/air temperature increases $PM_{10}$ concentrations by suppressing turbulent mixing. On average the strongest effect is observed in SB12 (green city with many planted trees) and SB15 (planting the most amount of trees) scenarios (Fig. 16), which show an increase of 24% and 21% in $PM_{10}$ with maxima over 30% in the late afternoon hours. Scenarios that simulate planting trees only in the Dělnická street, SB13 one tree alley in the center) and SB14 (tree alleys on both sides of the street), show similar responses in terms of the shape of the daily cycle, but with a lower overall increase (Fig. 16): on average, these scenarios show an increase of 5–14% in $PM_{10}$ concentrations, with maxima reaching almost 20% for SB14 and 10% for SB13 scenario (Fig. 16). Interestingly, over the perpendicular Komunardů street with no new trees planted, the concentrations tend to decrease throughout most of the day. The grey city scenarios SB10 and SB11 conversely show decreased $PM_{10}$ concentrations of around 20% in the afternoon and evening. Considering the spatial differences, the highest decrease is observed in the Komunardů street (over 50%; see Fig. 17).

## 4 Discussion and conclusions

In this work, we assessed the sensitivity of air and surface temperature, MRT, PET and $PM_{10}$ within the PALM model system 6.0 as a response to modification of basic surface material parameters as well as to common urbanistic strategies. For this we performed a set of semi-idealized model simulations for a diurnal cycle in a city quarter in Prague. The first set of scenarios,

https://doi.org/10.5194/gmd-2020-126
Preprint. Discussion started: 4 August 2020

Geoscientific Model Development
Discussions

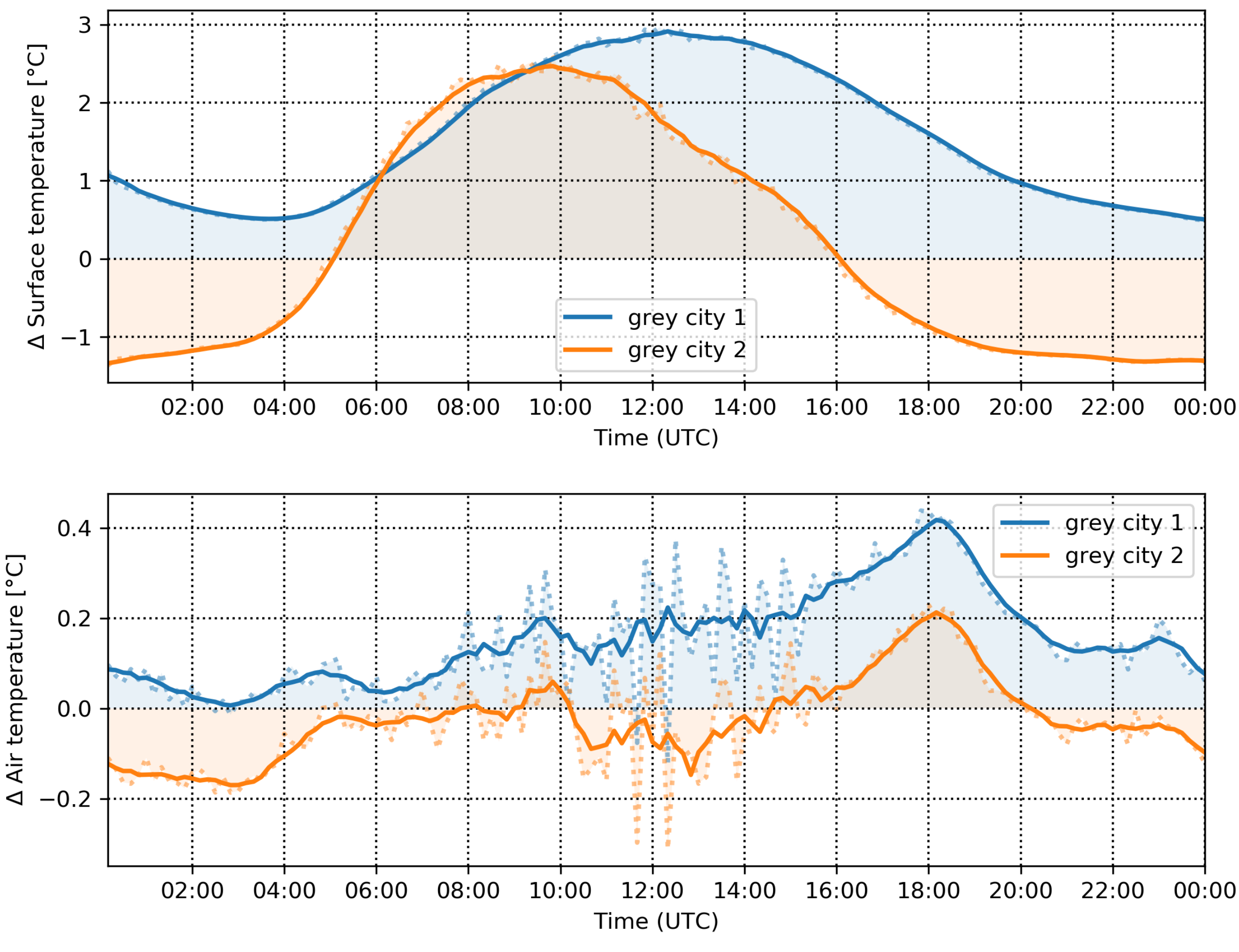


**Figure 12.** Domain-averaged differences in the surface temperature (top) and air temperature (bottom) for scenarios SB10 (blue) and SB11 (orange)

https://doi.org/10.5194/gmd-2020-126
Preprint. Discussion started: 4 August 2020


Geoscientific Model Development
Discussions
Open Access

**Table 4.** Differences in air temperature in the model first layer in K over the whole domain for SB scenarios (Scen): 24-hour (AVG) and 3-hour averages (00–03 to 21–24), minimum (MIN), maximum (MAX) and times (TIME).

| Scen | AVG | 00–03 | 03–06 | 06–09 | 09–12 | 12–15 | 15–18 | 18–21 | 21–24 | MIN | TIME | MAX | TIME |
|---|---|---|---|---|---|---|---|---|---|---|---|---|---|
| SB01 | 0.013 | 0.204 | 0.158 | -0.038 | -0.091 | -0.115 | -0.093 | -0.004 | 0.083 | -0.297 | 10:40 | 0.296 | 01:20 |
| SB02 | -0.013 | -0.149 | -0.125 | -0.007 | 0.072 | 0.080 | 0.100 | -0.010 | -0.067 | -0.190 | 03:00 | 0.318 | 11:50 |
| SB03 | 0.028 | 0.004 | 0.004 | 0.043 | 0.046 | 0.051 | 0.038 | 0.025 | 0.014 | -0.066 | 09:40 | 0.193 | 10:00 |
| SB04 | -0.017 | -0.013 | -0.016 | -0.027 | -0.020 | -0.025 | -0.015 | -0.011 | -0.007 | -0.137 | 13:50 | 0.120 | 10:20 |
| SB05 | 0.031 | 0.031 | 0.027 | 0.041 | 0.032 | 0.026 | 0.043 | 0.022 | 0.029 | -0.096 | 12:30 | 0.178 | 11:20 |
| SB06 | -0.041 | -0.012 | -0.024 | -0.044 | -0.049 | -0.084 | -0.052 | -0.037 | -0.029 | -0.249 | 10:10 | 0.076 | 11:00 |
| SB07 | -0.033 | -0.034 | -0.019 | -0.032 | -0.038 | -0.057 | -0.030 | -0.031 | -0.023 | -0.190 | 13:10 | 0.116 | 15:00 |
| SB09 | -0.253 | -0.214 | -0.164 | -0.189 | -0.308 | -0.326 | -0.272 | -0.308 | -0.247 | -0.455 | 12:20 | -0.105 | 05:20 |
| SB10 | 0.155 | 0.041 | 0.057 | 0.091 | 0.163 | 0.193 | 0.311 | 0.252 | 0.128 | -0.122 | 12:20 | 0.439 | 17:50 |
| SB11 | -0.025 | -0.153 | -0.068 | -0.013 | -0.027 | -0.042 | 0.096 | 0.060 | -0.050 | -0.312 | 12:20 | 0.229 | 18:00 |
| SB12 | -0.252 | -0.024 | -0.045 | -0.210 | -0.351 | -0.371 | -0.498 | -0.399 | -0.115 | -0.681 | 18:10 | 0.044 | 02:00 |
| SB13 | -0.051 | -0.013 | -0.017 | -0.039 | -0.066 | -0.079 | -0.090 | -0.070 | -0.036 | -0.172 | 13:10 | 0.077 | 10:00 |
| SB14 | -0.093 | -0.011 | -0.026 | -0.089 | -0.112 | -0.154 | -0.172 | -0.125 | -0.058 | -0.281 | 12:40 | 0.045 | 01:00 |
| SB15 | -0.122 | 0.002 | -0.027 | -0.118 | -0.162 | -0.188 | -0.240 | -0.172 | -0.068 | -0.364 | 12:20 | 0.078 | 01:20 |
| SB16 | 0.028 | -0.001 | 0.013 | 0.028 | 0.046 | 0.040 | 0.048 | 0.034 | 0.013 | -0.062 | 10:40 | 0.197 | 11:20 |
| SB17 | 0.025 | 0.000 | 0.006 | 0.028 | 0.029 | 0.023 | 0.046 | 0.042 | 0.022 | -0.075 | 09:00 | 0.122 | 10:50 |

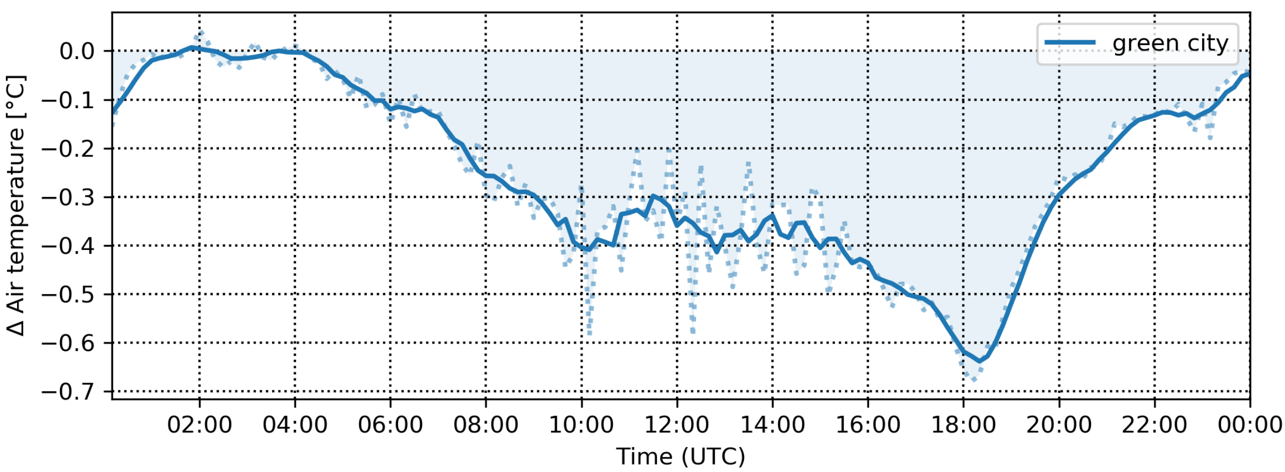


**Figure 13.** Domain-averaged differences in the air temperature for a green city scenario SB12 (blue)

https://doi.org/10.5194/gmd-2020-126
Preprint. Discussion started: 4 August 2020

Geoscientific Model Development
Discussions

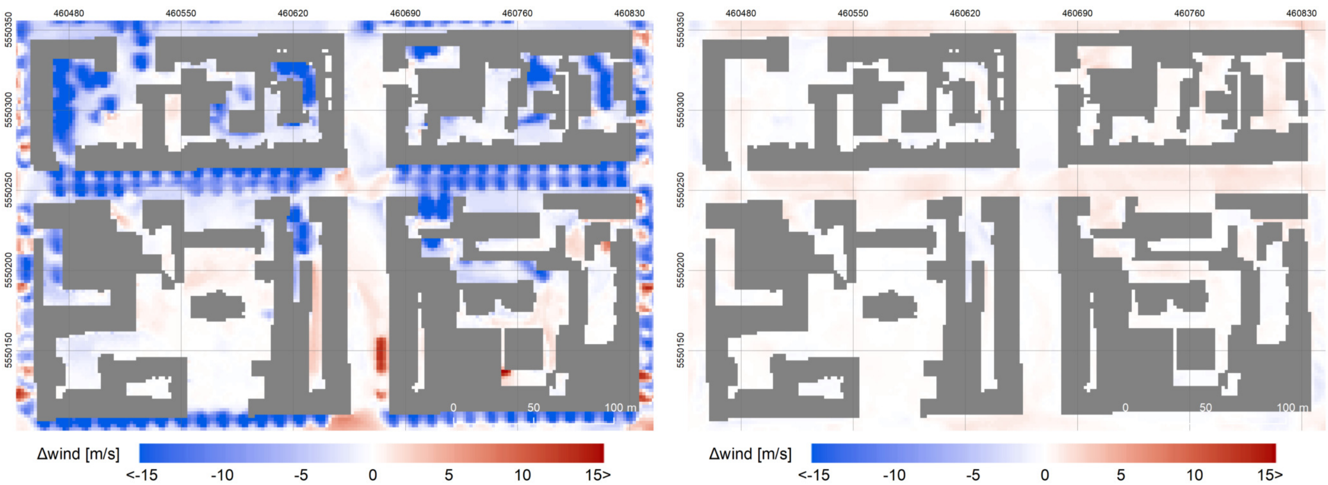


**Figure 14.** Example of spatio-temporal variability of 3-hour PET differences for a green city scenario SB12 at 09:00-12:00 UTC (left) and 21:00-24:00 UTC (right). EPSG: 32633, layer with roofs is own data source.

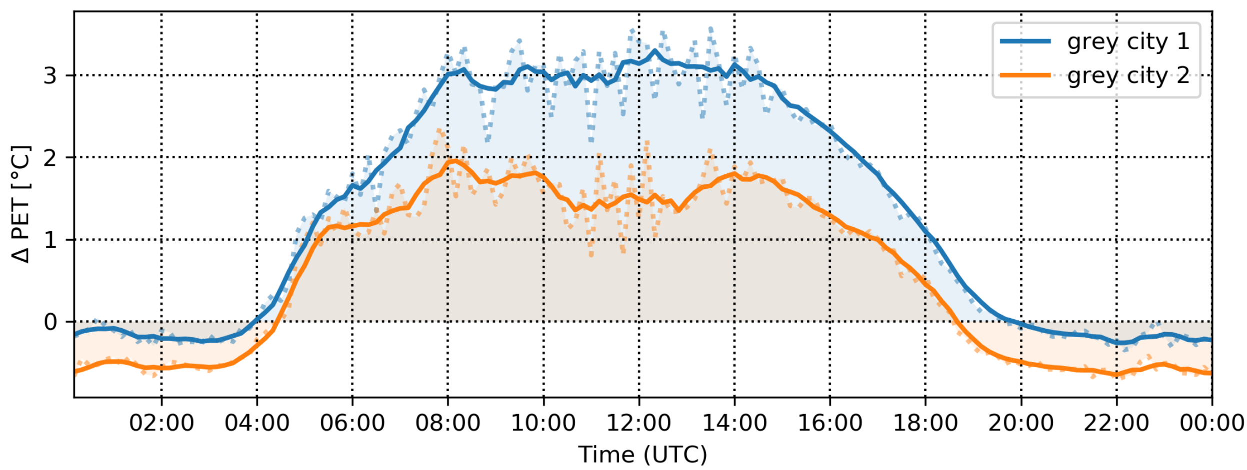


**Figure 15.** Domain-averaged differences in PET for a grey city scenarios SB10 (blue) and SB11 (orange)

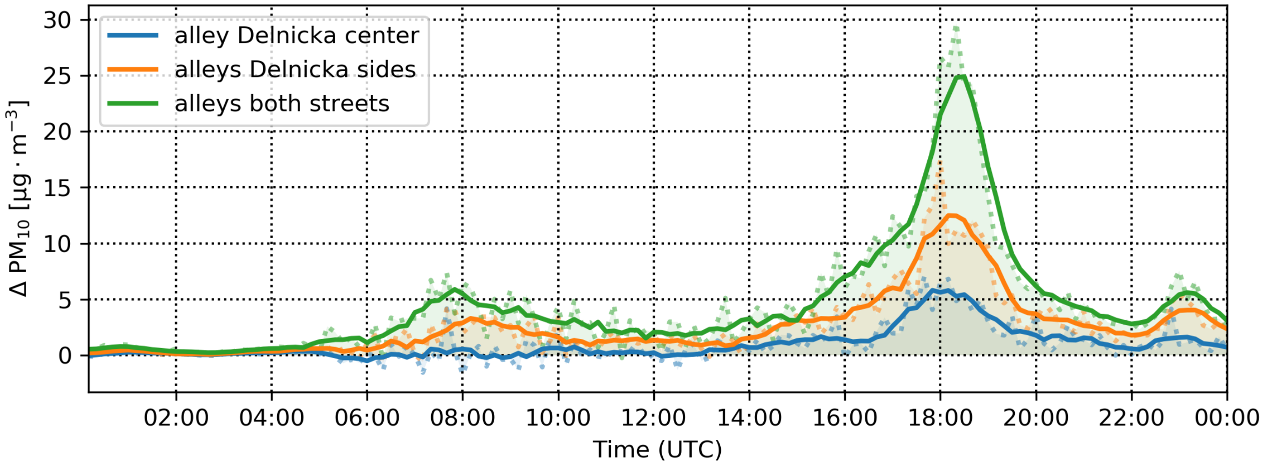


**Figure 16.** Domain-averaged differences in $PM_{10}$ for a new alley scenarios SB13 (blue), SB14 (orange) and SB15 (green)

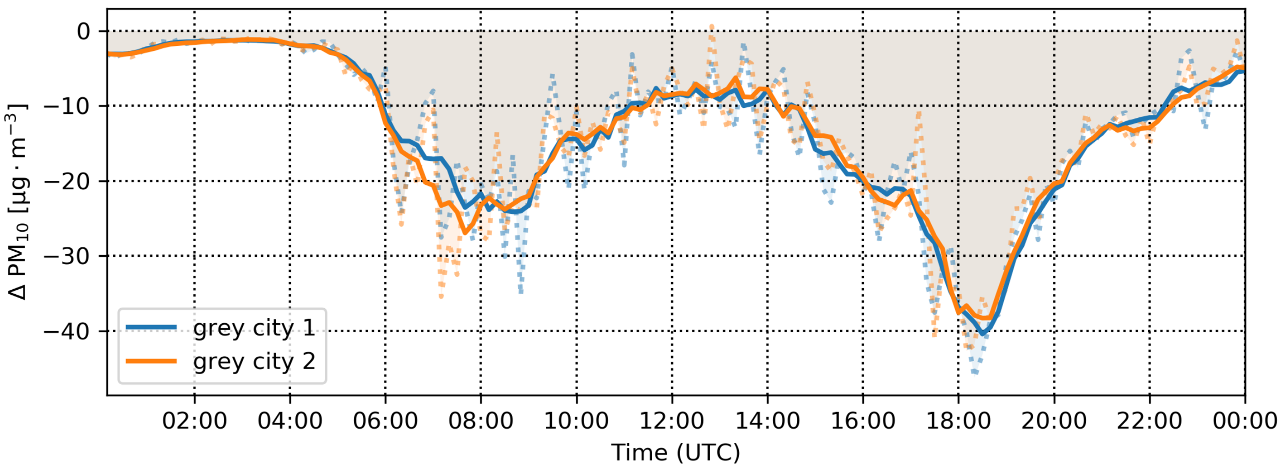


**Figure 17.** Differences in $PM_{10}$ for Komunardu street for a grey city scenarios SB10 (blue) and SB11 (orange)

https://doi.org/10.5194/gmd-2020-126
Preprint. Discussion started: 4 August 2020

Geoscientific Model Development Discussions

designed to examine the sensitivity to the parameter settings, shows the importance of the correct setting of the radiation parameters albedo and emissivity. This can be expected as the solar radiation is the main source of energy in the surface energy budget. Additionally, unlike some other parameters, radiation parameters are changed for all surfaces.

In addition to albedo and emissivity, thermal conductivity of walls and volumetric heat capacity of the materials play an important role. Other parameters show a limited average effect on the diurnal timescale, which, however, can be quite significant in some parts of the day, such as surface roughness in the morning hours and window fraction in the evening. Changing soil moisture by 20% is shown to be negligible overall in the context of the chosen domain (with only a small percentage of the surface covered by vegetation; see Table 1) except for surface temperature in the high-sun part of the day. Individual parts of the domain with larger coverage of vegetation show greater influence. Note that we investigated only the short-term response of the urban canopy on the outlined modifications. The trends might be more prominent if long-term storage of energy in the materials was considered, i.e., when simulating a full heat wave.

The second part of the sensitivity analysis focused on the UHI mitigation measures. One of the commonly considered measures is to paint surfaces white to increase surface albedo. However, our results indicate that this is only effective for lowering the surface and air temperature. In contrast, the biophysical indicators MRT and PET tend to be negatively affected, i.e., thermal comfort in the street is deteriorated due to increasing the amount of reflected radiation (note that the effect can be different on purely horizontal surfaces such as roofs). Improving both physical and biophysical temperature indicators requires application of other measures, such as urban greening at the same time. Similar findings have also been reported in e.g., Yang et al. (2015) who stress the need for precaution when adopting high-reflectivity surfaces or Aflaki et al. (2017) who found low-albedo vegetation effective for reducing mean radiant temperature.

Urban vegetation is found to be the most effective measure when considering reduction of both physical and biophysical temperature indicators. Conversely, grey city scenarios that reduce the amount of urban vegetation show significant worsening of the thermal comfort. Urban greenery is very often found an effective mitigation tool for UHI. However, some studies (e.g., Wang et al., 2016 or Makido et al., 2019) show that for the best effect it is necessary to combine several measures and also to consider that different parts of the city may need different measures.

One of the most important results of our analysis is that there is an opposite behaviour of thermal comfort and air quality indicators. Observed in both types of scenarios, the $PM_{10}$ concentrations typically increase with decreasing temperatures and vice versa. The main reason for this behaviour is decreased ventilation in the street canyon due to limited turbulent mixing and, in the case of adding urban greenery, also air flow blocking. However, in these simulations, only aerosols passive transfer was taken into account and thus the results may be different for other air quality indicators, e.g. when considering the influence of changing reaction coefficients and decrease of solar radiation for ozone chemistry.

In conclusion, this analysis shows that the proper setting of urban surface parameters is crucial for high-resolution LES models of the urban environment and that collecting this large amount of data is an essential part of the modelling technique. High temporal and spatial variability also shows the importance of using truly local information for each area of interest.

https://doi.org/10.5194/gmd-2020-126
Preprint. Discussion started: 4 August 2020

Geoscientific Model Development Discussions

### 4.1 Model limitations

This study applied the PALM model revision 4093. The model itself and its configuration have some limitations, with the following being the most important ones in our case:

- The model is configured without the PALM-4U building energy model (BEM) and the building inner temperature is considered constant (300 K) during the simulation. The impacts of the absence of a more complex indoor model differ in summer and winter seasons. In winter, assuming that the rooms are heated to the exact prescribed temperature by either direct local heat sources or by long-distance heating with the heating plant being outside the modelled domain, the model adds correct heat fluxes to the insides of the buildings, albeit not providing the amount of heating energy consumed among its outputs. In summer, the constant indoor temperature can be seen as a simplification for buildings without air conditioning where the wall insulation and wall heat capacity dampen most of the daily temperature difference, as long as the inner temperature is realistic and the daily total net heat flux is near zero. Buildings with air conditioning need a more complex indoor model with correctly placed heat exchangers (windows for individual A/C units and roofs for central A/C systems). For the simulated domain, there was no information available about the amount and placement of A/C systems, with the majority of the buildings being old apartment houses with presumably no central A/C systems and no visible individual A/C units at windows. For long term simulations, missing waste heat which could be provided by PALM's indoor model will be important. Given the short time scale of the present study simulations, the indoor model should not affect the outcome, though. The outer wall layers react very fast to changes in the surface energy balance, but the inner wall layers have large inertia so that nothing is likely to change if the indoor temperature changes in time.

- The model sensitivities are tested only during meteorological conditions of heat wave episodes as the main focus is on simulation of the UHI mitigation measures. Only the short-term response of the urban canopy was investigated. The behaviour, including long-term response, during other seasons and weather conditions can and probably will differ from presented results.

- The simulations do not consider any chemical reactions or aerosol dynamic processes of air pollutants, only the dispersion of traffic-related $PM_{10}$ is considered. Moreover, the boundary conditions of the chemical species on the parent domain were set to zero. This experiment design was selected as the focus of the study is on the sensitivity of the concentrations on the local conditions. The time needed for secondary organic aerosol (SOA) formation is much longer than the typical time the chemical species spent in the studied domain (e.g., Du et al., 2018 or Tang et al., 2018). The consequence is that the SOA concentration field is almost constant over the studied domain. It means that even though the SOA constitutes an important part of the $PM_{10}$, their omission does not change the differences of $PM_{10}$ between particular scenarios.

- This version initiates the building wall properties through the `building_2d` property in the model static driver, i.e., the wall properties are set to the roof grid cell over the wall (i.e. border grid cells of the roof). This leads to two simplifications:

https://doi.org/10.5194/gmd-2020-126
Preprint. Discussion started: 4 August 2020

Geoscientific Model Development Discussions

  - The properties of the wall can be set only in two height zones and the corner grid cells set the properties of two surface grid cells corresponding to different walls.
  - The roof properties in the border grid cells are initialized to the wall properties. This limitation leads to artefacts in roof and wall surface temperature and heat fluxes. This drawback was removed in later versions (model revision 4240 and later) by implementation of reading separate properties for individual surface cells from the new static driver variable building_surface_pars.

- The ventilation of very tight areas surrounded by high buildings is underestimated by the model and the concentrations of pollutants become unrealistically high in some circumstances. It is known that higher concentrations can be expected in enclosed spaces due to low turbulence (Gronemeier and Sühring, 2019). This problem was addressed in the model revision 4110. For the purpose of this analysis, these small areas were excluded from the evaluation.

*Code and data availability.* The PALM model system is freely available from http://palm-model.org (last access: 30 March 2020) and distributed under the GNU General Public Licence v3 (http://www.gnu.org/copyleft/gpl.html) , last access: 30 March 2020). The model source code of version 6.0 in revision r4093, used in this article is also available via https://doi.org/10.25835/0068421 (Geletic et al., 2020). Input data and additional outputs are available at http://hdl.handle.net/11104/0309669.

## Appendix A

### A1

*Author contributions.* MB was the main coordinator of manuscript proceedings and responsible for the general topic of paper and the analysis of results. All co-authors contributed to the manuscript text. KE configured and processed WRF simulations used for preparation of boundary conditions, JG was involved in geodata preprocessing, result postprocessing and data mining. JR and PK were strongly involved in PALM model setup and processed the PALM simulations, JR also participated in the experiment design. VF, FKS, MS and BM participated with the general topic, discussion and text preparation. NB, MA and MK are specialists in air quality modelling and participated in this field of study.

*Competing interests.* The authors declare that they have no conflict of interest.

*Acknowledgements.* The simulations were partly performed in the supercomputing centre IT4I which was supported by The Ministry of Education, Youth and Sports from the Large Infrastructures for Research, Experimental Development and Innovations project "IT4Innovations National Supercomputing Center – LM2015070" and partly on the HPC infrastructure of Institute of Computer Science supported by the long-term strategic development financing of the Institute of Computer Science (RVO:67985807).

https://doi.org/10.5194/gmd-2020-126
Preprint. Discussion started: 4 August 2020


Geoscientific Model Development Discussions

Financial support was provided by the *Operational Program Prague – Growth Pole of the Czech Republic* project "Urbanization of weather forecast, air-quality prediction and climate scenarios for Prague" (CZ.07.1.02/0.0/0.0/16_040/0000383) which is co-financed by EU. Coauthors BM, FK-S, and MS were supported by the Federal German Ministry of Education and Research (Germany) (grant no. 01LP1601A).

## References

Aflaki, A., Mirnezhad, M., Ghaffarianhoseini, A., Ghaffarianhoseini, A., Omrany, H., Wang, Z., Akbari, H.: Urban heat island mitigation strategies: A state-of-the-art review on Kuala Lumpur, Singapore and Hong Kong. Cities, 62, 131–145, https://doi.org/10.1016/j.cities.2016.09.003, 2017.

Ai, Z. T., Mak, C. M.: Modeling of coupled urban wind flow and indoor air flow on a high-density near-wall mesh: Sensitivity analyses and case study for single-sided ventilation. Environmental Modelling & Software, 60, 57–68, https://doi.org/10.1016/j.envsoft.2014.06.010, 2014.

Arnfield, A. J.: Two decades of urban climate research: a review of turbulence, exchanges of energy and water, and the urban heat island. International Journal of Climatology: a Journal of the Royal Meteorological Society, 23, 1, 1–26, https://doi.org/10.1002/joc.859, 2003.

Ashie, Y., Kono, T.: Urban-scale CFD analysis in support of a climate-sensitive design for the Tokyo Bay area. International Journal of Climatology, 31, 174–188, https://doi.org/10.1002/joc.2226, 2010.

Deardorff, J. W.: Stratocumulus-capped mixed layers derived from a three-dimensional model, Boundary-Layer Meteorol., 18, 495–527, 1980.

Du, Z., Hu, M., Peng, J., Zhang, W., Zheng, J., Gu, F., Qin, Y., Yang, Y., Li, M., Wu, Y., Shao, M., and Shuai, S.: Comparison of primary aerosol emission and secondary aerosol formation from gasoline direct injection and port fuel injection vehicles, Atmos. Chem. Phys., 18, 9011–9023, https://doi.org/10.5194/acp-18-9011-2018, 2018.

Ebi, K.: Climate change and health risks: assessing and responding to them through "adaptive management". Health Affairs, 30, 5, 924–930, https://doi.org/10.1377/hlthaff.2011.0071, 2011.

Emmanuel, R., Loconsole, A.: Green infrastructure as an adaptation approach to tackling urban overheating in the Glasgow Clyde Valley Region, UK. Landscape and Urban Planning, 138, 71–86, https://doi.org/10.1016/j.landurbplan.2015.02.012, 2015.

Geletic, J. et al.: Dataset: PALM 6.0 r4093. https://doi.org/10.25835/0068421, 2020.

Gill, S., Handley, J., Ennos, A., and Pauleit, S.: Adapting cities for climate change: the role of the green infrastructure. Built Environment, 33, 1, 115–133, https://doi.org/10.2148/benv.33.1.115, 2007.

Gronemeier, T. and Sühring, M.: On the Effects of Lateral Openings on Courtyard Ventilation and Pollution—A Large-Eddy Simulation Study, Atmosphere 10(2), 63, https://doi.org/10.3390/atmos10020063, 2019.

Gross, G.: Effects of different vegetation on temperature in an urban building environment. Micro-scale numerical experiments. Meteorologische Zeitschrift, 21, 4, 399–412(14), https://doi.org/10.1127/0941-2948/2012/0363, 2012.

Hackbusch, W.: Multi-Grid Methods and Applications. Springer, Berlin, Heidelberg, 2nd printing, https://doi.org/10.1007/978-3-662-02427-0, 1985.

Haines, A., Kovats, R. S., Campbell-Lendrum, D., and Corvalan, C.: Climate change and human health: impacts, vulnerability and public health. Public Health, 120, 7, 585-596, https://doi.org/10.1016/j.puhe.2006.01.002, 2006.

Heldens, W., Burmeister, C., Kanani-Sühring, F., Maronga, B., Pavlik, D., Sühring, M., Zeidler, J., and Esch, T.: Geospatial input data for the PALM model system 6.0: model requirements, data sources, and processing, Geosci. Model Dev. Discuss., https://doi.org/10.5194/gmd-2019-355, in review, 2020.

Hunt, A., and Watkiss, P.: Climate change impacts and adaptation in cities: a review of the literature. Climatic Change, 104, 1, 13–49, https://doi.org/10.1007/s10584-010-9975-6, 2011.

https://doi.org/10.5194/gmd-2020-126
Preprint. Discussion started: 4 August 2020



IPCC: Climate Change 2014: Impacts, Adaptation, and Vulnerability. Part A: Global and Sectoral Aspects. Contribution of Working Group II to the Fifth Assessment Report of the Intergovernmental Panel on Climate Change, edited by: Field, C. B., Barros, V. R., Dokken, D. J., Mach, K. J., Mastrandrea, M. D., Bilir, T. E., Chatterjee, M., Ebi, K. L., Estrada, Y. O., Genova, R. C., Girma, B., Kissel, E. S., Levy, A. N., MacCracken, S., Mastrandrea, P. R., and White, L. L., Cambridge University Press, Cambridge, United Kingdom and New York, NY, USA, 1132 pp., https://doi.org/10.1017/CBO9781107415379, 2014a.

IPCC: Climate Change 2014: Mitigation of Climate Change. Contribution of Working Group III to the Fifth Assessment Report of the Intergovernmental Panel on Climate Change, edited by: Edenhofer, O., Pichs-Madruga, R., Sokona, Y., Farahani, E., Kadner, S., Seyboth, K., Adler, A., Baum, I., Brunner, S., Eickemeier, P., Kriemann, B., Savolainen, J., Schlömer, S., von Stechow, C., Zwickel, T., and Minx, J. C., Cambridge University Press, Cambridge, United Kingdom and New York, NY, USA, https://doi.org/10.1017/CBO9781107415416, 2014b.

Kovats, R. S., and Hajat, S.: Heat stress and public health: a critical review. Annual Review of Public Health, 29, 41–55, https://doi.org/10.1146/annurev.publhealth.29.020907.090843, 2008.

Krč, P., Resler, J., Fuka, V., Sühring, M., Salim, M., Schubert, S.: Radiative Transfer Model 3.0 integrated into the PALM model system 6.0. submitted to GMD

Lobaccaro, G., Acero, J. A.: Comparative analysis of green actions to improve outdoor thermal comfort inside typical urban street canyons. Urban Climate, 14, 2, 251–267, https://doi.org/10.1016/j.uclim.2015.10.002, 2015.

Makido, Y., Hellman, D., Shandas, V.: Nature-Based Designs to Mitigate Urban Heat: The Efficacy of Green Infrastructure Treatments in Portland, Oregon. Atmosphere, 10, 282, https://doi.org/10.3390/atmos10050282, 2019.

Maronga, B., Banzhaf, S., Burmeister, C., Esch, T., Forkel, R., Fröhlich, D., Fuka, V., Gehrke, K. F., Geletič, J., Giersch, S., Gronemeier, T., Groß, G., Heldens, W., Hellsten, A., Hoffmann, F., Inagaki, A., Kadasch, E., Kanani-Sühring, F., Ketelsen, K., Khan, B. A., Knigge, C., Knoop, H., Krč, P., Kurppa, M., Maamari, H., Matzarakis, A., Mauder, M., Pallasch, M., Pavlik, D., Pfafferott, J., Resler, J., Rissmann, S., Russo, E., Salim, M., Schrempf, M., Schwenkel, J., Seckmeyer, G., Schubert, S., Sühring, M., von Tils, R., Vollmer, L., Ward, S., Witha, B., Wurps, H., Zeidler, J., and Raasch, S.: Overview of the PALM model system 6.0, Geosci. Model Dev., 13, 1335–1372, https://doi.org/10.5194/gmd-13-1335-2020, 2020.

Maronga, B., Gryschka, M., Heinze, R., Hoffmann, F., Kanani-Sühring, F., Keck, M., Ketelsen, K., Letzel, M. O., Sühring, M., and Raasch, S.: The Parallelized Large-Eddy Simulation Model (PALM) version 4.0 for atmospheric and oceanic flows: model formulation, recent developments, and future perspectives, Geosci. Model Dev., 8, 2515–2551, https://doi.org/10.5194/gmd-8-2515-2015, 2015.

MEFA 13, User guide, Prague, May 2013, downloadable from http://www.atem.cz/ke_stazeni.php (software and user guide documentation in Czech language only). Accessed on 21.03.2020.

Mills, G.: Urban climatology: History, status and prospects. Urban Climate, 10, 3, 479–489, https://doi.org/10.1016/j.uclim.2014.06.004, 2014.

Moeng, C.-H. and Wyngaard, J. C.: Spectral analysis of large-eddy simulations of the convective boundary layer, Journal of the Atmospheric Sciences, 45, 3573–3587, https://doi.org/10.1175/1520-0469(1988)045<3573:SAOLES>2.0.CO;2, 1988.

Müller, N., Kuttler, W., and Barlag, A. B.: Counteracting urban climate change: adaptation measures and their effect on thermal comfort. Theoretical and Applied Climatology, 115, 243–257, https://doi.org/10.1007/s00704-013-0890-4, 2013.

Oke, T. R.: The energetic basis of the urban heat island. Q. J. Roy. Meteor. Soc., 108, 1–24, https://doi.org/10.1002/qj.49710845502, 1982.

Patz, J. A., Campbell-Lendrum, D., Holloway, T., and Foley, J. A.: Impact of regional climate change on human health. Nature, 438, 7066, 310–317, https://doi.org/10.1038/nature04188, 2005.

https://doi.org/10.5194/gmd-2020-126
Preprint. Discussion started: 4 August 2020


Geoscientific
Model Development
Discussions

Resler, J., Krč, P., Belda, M., Juruš, P., Benešová, N., Lopata, J., Vlček, O., Damašková, D., Eben, K., Derbek, P., Maronga, B., and Kanani-Sühring, F.: PALM-USM v1.0: A new urban surface model integrated into the PALM large-eddy simulation model. Geosci. Model Dev., 10, 3635–3659, https://doi.org/10.5194/gmd-10-3635-2017, 2017.

Ramponi, R., Blocken, B.: CFD simulation of cross-ventilation for a generic isolated building: Impact of computational parameters. Building and Environment, 53, 34–48, https://doi.org/10.1016/j.buildenv.2012.01.004, 2012.

Saiki, E. M., Moeng, C.-H., and Sullivan, P. P.: Large-eddy simulation of the stably stratified planetary boundary layer, Bound. Lay.-Meteorol., 95, 1–30, https://doi.org/10.1023/A:1002428223156, 2000.

Souch, C., and Grimmond, S.: Applied climatology: urban climate. Progress in Physical Geography, 30, 2, 270-279, https://doi.org/10.1191/0309133306pp484pr, 2006.

Stewart, I. D.: A systematic review and scientific critique of methodology in modern urban heat island literature. International Journal of Climatology, 31, 2, 200–217, https://doi.org/10.1002/joc.2141, 2011.

Su, W., Zhang, Y., Yang, Y., Ye, G.: Examining the Impact of Greenspace Patterns on Land Surface Temperature by Coupling LiDAR Data with a CFD Model. Sustainability, 6, 10, 6799–6814, https://doi.org/10.3390/su6106799, 2014.

Tang, R., Wu, Z., Li, X., Wang, Y., Shang, D., Xiao, Y., Li, M., Zeng, L., Wu, Z., Hallquist, M., Hu, M., and Guo, S.: Primary and secondary organic aerosols in summer 2016 in Beijing, Atmos. Chem. Phys., 18, 4055–4068, https://doi.org/10.5194/acp-18-4055-2018, 2018.

Wang, Y., Berardi, U., Akbari, H.: Comparing the effects of urban heat island mitigation strategies for Toronto, Canada. Energy and Buildings, 114, 2–19, https://doi.org/10.1016/j.enbuild.2015.06.046, 2016.

Wicker, L. J., and Skamarock, W. C.: Time-Splitting Methods for Elastic Models Using Forward Time Schemes. Monthly Weather Review, 130, 2088–2097, https://doi.org/10.1175/1520-0493(2002)130<2088:TSMFEM>2.0.CO;2, 2002.

Yang, J., Wang, Z., Kaloush, K. E.: Environmental impacts of reflective materials: Is high albedo a 'silver bullet' for mitigating urban heat island? Renewable and Sustainable Energy Reviews, 47, 830–843, https://doi.org/10.1016/j.rser.2015.03.092, 2015.

Zanobetti, A., O'Neill, M. S., Gronlund, C. J., and Schwartz, J. D.: Summer temperature variability and long-term survival among elderly people with chronic disease. Proceedings of the National Academy of Sciences of the United States of America, 109, 17, 6608–6613, https://doi.org/10.1073/pnas.1113070109, 2012.

Žák, M., Zahradníček, P., Skalák, P., Halenka, T., Aleš, D., Fuka, V., Kazmuková, M., Zemánek, O., Flegl, J., Kiesel, K., Jareš, R., Resler, J., Huszár, P.: Pilot Actions in European Cities – Prague. In: Musco F. (eds) Counteracting Urban Heat Island Effects in a Global Climate Change Scenario. Springer, Cham, 373–400, https://doi.org/10.1007/978-3-319-10425-6_14, 2016